DEUTSCHES ELEKTRONEN-SYNCHROTRON DESY

DESY 80/90
September 1980

JET CROSS SECTIONS IN LEPTOPRODUCTION FROM QCD

by

Ch. Rumpf, G. Kramer and J. Willrodt
II. Institut für Theoretische Physik der Universität Hamburg

NOTKESTRASSE 85 · 2 HAMBURG 52

To be sure that your preprints are promptly included in the
HIGH ENERGY PHYSICS INDEX ,
send them to the following address (if possible by air mail) :

DESY
Bibliothek
Notkestrasse 85
2 Hamburg 52
Germany

DESY 80/90
September 1980

Jet Cross Sections in Leptoproduction from QCD [+)]

by

Ch. Rumpf [*)], G. Kramer and J. Willrodt

II. Institut für Theoretische Physik der Universität, Hamburg

Abstract

We have calculated the longitudinal and other polarization dependent cross sections for jet production in deep inelastic ep, νp and $\bar{\nu}$p scattering up to order α_s of the quark-gluon coupling constant. Fragmentation of final state partons into hadrons is taken into account. Distributions in thrust, p^2_{Tin} and p^2_{Tout} are predicted for all three reactions and various values of W and Q.

[+)] Supported by Deutsche Forschungsgemeinschaft
Grant Kr 671/1

[*)] Now at Siemens AG, München

1. Introduction

In lowest order Quantum Chromodynamics (QCD) the final state in deep inelastic lepton-nucleon scattering consists of two jets: one originating from the struck quark and the other arising from the fragments of the target nucleon from which the quark was emitted. In the next order of QCD three jet events must occur, in which, for example, the outgoing quark radiates a gluon with high transverse momentum, thereby producing a third jet of hadrons [1]. The study of three-, four- and multi-jet production is an important test of QCD perturbation theory beyond the leading logarithm approximation which was applied so far in the analysis of the total deep inelastic cross section.

Presumably the cleanest way to study QCD jets is in e^+e^- annihilation into hadrons. Here the initial state is purely leptonic so that the non-perturbative mechanism which converts quarks and gluons into observable hadrons acts only in the final state. After the discovery of three-jet events in e^+e^--annihilation [2] direct confrontation of QCD predictions with experimental results have been reported [3]. It is clear that such tests of QCD perturbation theory must be made also for other processes. Deep inelastic lepton-nucleon scattering is well suited for this purpose. Although the non-perturbative effects play a role both in the initial and final states the momentum distribution of the ingoing quark or gluon can in principle be determined from measurements of the total inclusive cross section. With this information on hand one can predict the jet properties in a similar way as it was done for e^+e^- annihilation. A variety of such predictions are already available [4].

Unfortunately in all this work the final hadronization of quarks and gluons was not taken into account. It is well known now from calculations of jet properties in e^+e^- annihilation that the smearing in transverse momentum due to the hadronization process is very important [3]. It is the purpose of this work to take this into account also in deep inelastic ℓp scattering [5].

We do this for the total unpolarized jet production cross section, for the longitudinal cross section and for jet asymmetries which have been computed in the tree-graph approximation in some earlier work [6]. The lepton-proton (ep, νp and $\bar{\nu}$p) scattering is calculated in the center-of-mass frame of the outgoing hadrons. Then in lowest order we have the back-to-back jets of quark and diquark and in higher order three jets. In this frame the kinematic situation

is very similar to e^+e^- annihilation. In the experiment the frame will be different. Either the lepton is scattered on a fixed target or lepton and proton have rather different energies with opposite directed momenta as in the planned ep storage ring HERA. It is easy to calculate the consequences of the model considered in this paper in these other frames. This has been done partly in connection with working out proposals for experiments with HERA [7] . We have chosen the hadron center-of-mass frame for reasons of simplicity and in order to present an overview of the results of the model.

Our paper is organized in the following way. In section 2, we collect all the necessary formulae corresponding to the Feynman graphs which give two current jets and to the phenomenological description of structure functions. Here we give also the results for ep, νp and $\bar{\nu}$p scattering. These results are similar to our earlier work [6] but include now also νp and $\bar{\nu}$p. In section 3 we describe the model used for the final hadronization process. We compare some results for two-jet production with recent experimental data for νp and $\bar{\nu}$p production at low energies (W $\lesssim$ 10 GeV) [F1] in order to test the fragmentation model. In section 4 we present the results including final hadronization. All results are given for the final hadron center-of-mass frame. Our findings and their experimental consequences are summarized in section 5.

2. Cross-Sections for Parton Production

In leptoproduction, the parton cross-section in the first order of perturbation theory is expressed in terms of the usual kinematical variables:

$$Q^2 = -q^2 \;,\quad y = \frac{pq}{p\cdot l} \;,\quad z = \frac{p\cdot p_1}{p\cdot q} \;,\quad x = \frac{Q^2}{2pq} \quad \text{and} \quad \varphi$$

where p , p_1, l and q are defined in Fig. 1a and φ is the angle between l_T (transverse with respect to $\vec{q}$) and $\vec{p}_1$ (see Fig. 2). The general formula for the differential parton cross-section for the process $e^- + p \to e^- + p_1 + p_2$ in the one-photon approximation, where p is the momentum of the incoming parton a, is

$$d\sigma^a = \frac{\alpha^2}{32\pi^2 Q^4}\, l^{\mu\nu} T_{\mu\nu}\, y\, \delta\left(\vec{p}_{1T}^{\,2} - Q^2 \frac{z}{x}(1-x)(1-z)\right) dp_{1T}^2\, dx\, dy\, dz\, d\varphi \tag{2.1}$$

where $l_{\mu\nu}$ is the lepton tensor:

$$l_{\mu\nu} = 2\left[l_\mu l'_\nu + l_\mu' l_\nu - l l' g_{\mu\nu}\right] \tag{2.2}$$

and $T_{\mu\nu}$ is the hadron tensor.

We have three contributions to the process e^- + proton $\to e^- + p_1 + p_2$ up to order $\alpha_s = g^2/4\pi$: $\gamma_v + q \to q + g$ (Fig. 1b), $\gamma_v + g \to q + \bar{q}$ (Fig. 1c) and $\gamma_v + \bar{q} \to \bar{q} + g$ (Fig. 1d). The hadronic tensor for the first process is:

$$\begin{aligned} T_{\mu\nu} = 4c_2 Q_a^2 g^2 \Big\{ & \frac{1}{p_1\cdot p_2}\left[\{p,p_1\}_{\mu\nu} + \{p_1,p_1\}_{\mu\nu} + \{p,p_2\}_{\mu\nu}\right] \\ & + \frac{1}{p\cdot p_2}\left[\{p_1,p_2\}_{\mu\nu} - \{p,p\}_{\mu\nu} - \{p,p_1\}_{\mu\nu}\right] \\ & + \frac{p\cdot p_1}{p\cdot p_2\; p_1\cdot p_2}\left[2\{p,p_1\}_{\mu\nu} - \{p_1,p_2\}_{\mu\nu} + \{p,p_2\}_{\mu\nu}\right]\Big\} \end{aligned} \tag{2.3}$$

where Q_f is the charge of the quark and c_2 is the colour factor $c_2 = \frac{4}{3}$.

This formula is for massless quarks. The hadronic tensor for the second process ($\gamma_v + g \to q + q$) in the notation of Fig. 1c is instead:

$$T_{\mu\nu} = 4c_3 Q_a^2 g^2 \left\{ \frac{1}{p_1 p_2} \left[\{p,p_1\}_{\mu\nu} + \{p_1,p_2\}_{\mu\nu} + \{p_2,p_2\}_{\mu\nu} \right] \right.$$
$$+ \frac{1}{p \cdot p_1} \left[\{p,p_2\}_{\mu\nu} + \{p_1,p_2\}_{\mu\nu} + \{p_3,p_1\}_{\mu\nu} \right]$$
$$\left. + \frac{p_1 p_2}{p \cdot p_1 \; p \cdot p_2} \left[-2\{p_1,p_2\}_{\mu\nu} + \{p,p_1\}_{\mu\nu} + \{p,p_2\}_{\mu\nu} \right] \right\} \quad (2.4)$$

with $c_3 = \frac{1}{2}$ and $\{p_1, p_2\}^{\mu\nu} = p_1^\mu p_2^\nu + p_2^\mu p_1^\nu - g^{\mu\nu} p_1 \cdot p_2$.
The tensor for the third contribution ($\gamma_v + \bar{q} \to \bar{q} + g$) is identical to the tensor of the first process (2.3).

The one-parton inclusive cross section for the lepton scattering on a nucleon is then simply obtained by integration over the incident parton variable x[9]:

$$\frac{d\sigma}{dx_B\, dy\, dz\, d\varphi} = \sum_a \int d\eta \int dx \; \delta(x_B - \eta x) \, f_a(\eta, Q^2) \frac{d\sigma^a}{dx\, dy\, dz\, d\varphi} \quad (2.5)$$

where $f_a(\eta, Q^2)$ is the probability distribution of parton a (quark, antiquark or gluon) with a fraction of momentum η, i.e. $p = \eta P$ (see Fig. 1e) and $x_B = \frac{Q^2}{2Pq}$ with P being the nucleon four-momentum.

Actually we are interested in the three-jet cross section. The three jets in the final state are quark and gluon (Fig. 1b) or quark and antiquark (Fig. 1c) or antiquark and gluon (Fig. 1d) with momenta p_1 and p_2 and the diquark jet with momentum p_3. We go into the final hadronic rest system $\vec{P} + \vec{q} = 0$ and use as variables $W^2 = (P + q)^2$, Q^2 and $x_i = 2p_{i0}/W$ with the constraint $x_1 + x_2 + x_3 = 2$ (see Fig. 1e for the notation of momenta). All partons are massless. The variables x_i are related to z and η by:

$$x_1 = 1 - x_3(1 - z)$$
$$x_3 = \frac{1-\eta}{1-x_B} = (1-\eta)\frac{W^2+Q^2}{W^2} \quad (2.6)$$

The y and φ dependence of the three-jet cross section can be separated by introducing polarization dependent cross sections [10] . For lepton-nucleon scattering (in the one-photon approximation) the decomposition has the following form [6]

$$\frac{d\sigma}{dQ^2 dW^2 d\varphi\, dx_1 dx_2} = \Gamma \left\{ \frac{d\sigma_U}{dx_1 dx_2} + \frac{2(1-y)}{1+(1-y)^2} \frac{d\sigma_L}{dx_1 dx_2} \right. \quad (2.7)$$
$$\left. + \frac{2(1-y)}{1+(1-y)^2} \cos 2\varphi \frac{d\sigma_T}{dx_1 dx_2} - \frac{(1-y)^{1/2}(2-y)}{1+(1-y)^2} \cos\varphi \frac{d\sigma_I}{dx_1 dx_2} \right\}$$

Γ is the equivalent photon spectrum

$$\Gamma = \frac{\alpha W^2}{4\pi^2 Q^2 (W^2+Q^2)^2} \left(1 + (1-y)^2\right) \quad (2.8)$$

The term $d\sigma_U$ is the cross section for unpolarized transverse virtual photons, $d\sigma_T$ is due to the transverse linear polarization of the photon, $d\sigma_L$ accounts for the longitudinal photons and $d\sigma_I$ describes the interference of the longitudinal and transverse matrix element.

The total cross section is written in the form

$$\frac{d\sigma}{dQ^2 dW^2 d\varphi} = \Gamma \sigma_U \quad (2.9)$$

In zeroth order σ_U (see Fig. 1f) is

$$\sigma_U^0 = \frac{\pi e^2 Q_a^2}{W^2} f_a(x_B, Q^2) \quad (2.10)$$

We recall $x_B = Q^2/(W^2 + Q^2)$.

The derivation of the three-jet cross section formula is rather lengthy. We expressed $l_{\mu\nu} T^{\mu\nu}$ in (2.1) directly in terms of x_1, x_2 and x_3 with $T_{\mu\nu}$ given by (2.3) or (2.4) and substituted this into (2.5). The differentials $dyd\eta$ were transformed into $dW^2 dQ^2$ and $dzdx_B$ into $dx_1\, dx_2$. For the diagrams in Fig. 1b and Fig. 1d we obtained:

$$(\sigma_u^0)^{-1}\frac{d\sigma_u}{dx_1\,dx_2} = \frac{C_1}{x_{11}\,x_{13}\,x_3}\left\{\frac{W^2}{\eta(W^2+Q^2)}\,x_{13}^2\,(x_{11}^2+x_{12}^2) + x_{11}\,x_{13}\,(x_{12}+x_3) + \frac{Q^2}{W^2}\,(x_{12}^2+x_3^2)\right\}$$

$$(\sigma_u^0)^{-1}\frac{d\sigma_L}{dx_1\,dx_2} = 2(\sigma_u^0)^{-1}\frac{d\sigma_T}{dx_1\,dx_2} = \frac{4C_1Q^2x_{12}}{\eta(W^2+Q^2)\,x_3} \qquad (2.11)$$

$$(\sigma_u^0)^{-1}\frac{d\sigma_I}{dx_1\,dx_2} = \frac{4C_1}{x_3}\left(\frac{x_{12}\,x_{13}\,Q^2}{x_{11}\,W^2}\right)^{1/2}\left\{\frac{W^2}{\eta(W^2+Q^2)}(x_1-x_2) - \frac{x_{12}}{x_{13}}\right\}$$

where $x_{1i} = 1 - x_i$ ($i = 1,2,3$) and C_1 is a factor universal to all four partial cross-sections:

$$C_1 = \frac{W^2}{\eta(W^2+Q^2)\,x_3}\;\frac{fa(\eta,Q^2)}{fa(x_8,Q^2)}\;c_1\frac{\alpha_s}{2\pi} \qquad (2.12)$$

In these formulae we assumed that $p_T = 0$. For diagram Fig. 1c, where the parton a is the gluon, the corresponding formulae are:

$$(\sigma_u^0)^{-1}\frac{d\sigma_u}{dx_1\,dx_2} = \frac{C_3}{x_{11}\,x_{12}}\;\frac{W^4x_{13}^2+Q^4}{\eta^2(W^2+Q^2)^2}\;(x_{11}^2+x_{12}^2)$$

$$(\sigma_u^0)^{-1}\frac{d\sigma_L}{dx_1\,dx_2} = 2(\sigma_u^0)^{-1}\frac{d\sigma_T}{dx_1\,dx_2} = \frac{8C_3Q^2W^2x_{13}}{\eta^2(W^2+Q^2)^2} \qquad (2.13)$$

$$(\sigma_u^0)^{-1}\frac{d\sigma_I}{dx_1\,dx_2} = 4C_3\frac{Q^2W^2}{\eta^2(W^2+Q^2)^2}\left(\frac{Q^2x_{13}}{W^2x_{11}x_{12}}\right)^{1/2}(x_1-x_2)\left(\frac{W^2}{Q^2}x_{13}-1\right)$$

c_3 deviates from c_1 just by the colour factors: $c_3 = \frac{C_3}{C_1}\,c_1$.
In the final expression, where all three contributions of Fig. 1b, c and d are added, the normalization is given by (2.10) with a sum over quark and antiquark contributions.

We remark that in the leading logarithm approximation, i. e. $x_2 \to 0$ or $x_1, x_3 \to 1$, the quark and antiquark contributions (2.11) dominate over the gluon contribution (2.13).

Concerning the two-jet contribution we give only some estimates and approximate formulas in this section in order to show its order of magnitude in comparison with the three-jet contribution. A more detailed calculation of the two-jet

cross section based on a Feynman-Field type fragmentation model is described in the next section. In lowest order QCD the two-jet cross section is obtained from the diagram in Fig. 1f. If it is assumed that the parton leaves the proton with no transverse momentum, i.e. $P = \eta\,p$, the contribution of Fig. 1f to σ_L, σ_T and σ_I vanishes [11] . To obtain a realistic estimate of the non-perturbative terms to σ_L and the azimuthal asymmetries we shall take into account the primordial transverse momentum in the structure function of the proton. Let p_T be the transverse momentum of the parton when leaving the nucleon (this is equal to the transverse momentum of the outgoing quark), then we have the following contributions to the various cross sections from the lowest order tree-graph in Fig. 1f [11]

$$(\sigma_u^0)^{-1}\frac{d\sigma_u^0}{dx_1\,dx_2} = \delta(1-x_1)\,\delta(1-x_2)$$

$$(\sigma_u^0)^{-1}\frac{d\sigma_L^0}{dx_1\,dx_2} = 2(\sigma_u^0)^{-1}\frac{d\sigma_T}{dx_1\,dx_2} = \frac{4p_T^2}{Q^2}\,\delta(1-x_1)\,\delta(1-x_2) \qquad (2.14)$$

$$(\sigma_u^0)^{-1}\frac{d\sigma_I^0}{dx_1\,dx_2} = \frac{4p_T}{(Q^2)^{1/2}}\,\delta(1-x_1)\,\delta(1-x_2)$$

In (2.14) the p_T is measured with respect to the momentum $\vec{q}$ of the virtual photon. In the derivation of the formulas we assumed the quarks to be on mass shell with $m = 0$ [F2] . For p_T we assumed the value 0.4 GeV. For increasing Q^2 σ_L vanishes like $1/Q^2$ and σ_I like $1/(Q^2)^{1/2}$, which must be compared to $\alpha_s(Q^2) \sim \ln^{-1} Q^2$ which determines the three-jet contributions. The σ_I term is comparable in magnitude to the QCD term even at $Q^2 \simeq 100\ \mathrm{GeV}^2$. However, this term drops out in the case that we do not distinguish the current jet from the target jet as will be assumed in the following if not stated otherwise.

The variables x_1, x_2 and x_3 are transformed into jet variables, for example, thrust T and spherocity S. They are related to x_1, x_2 and x_3 by [13]

$$T = \max\,(x_1, x_2, x_3) \qquad (2.15)$$

$$S = \frac{64}{\pi^2}\,(1-x_1)\,(1-x_2)\,(1-x_3)\,/\,T^2 \qquad (2.16)$$

For $x_1 > x_2 > x_3$ we have

$$dx_1\,dx_2 = \frac{\pi^2\,T\,dT\,dS}{64(1-T)\left(1-\pi^2S/16(1-T)\right)^{1/2}} \qquad (2.17)$$

In order to compute $d\sigma/dTdS$ we sum over the six regions of phase space $x_1 > x_2 > x_3$ etc. which consist of the six permutations of 1,2,3. Then the double differential distributions for $d\sigma_u$, $d\sigma_L$, $d\sigma_T$ and $d\sigma_I$ are integrated over S.

Since the structure functions $f_a(x, Q^2)$ are known from experiment only for a limited range of Q^2 we must compute them for the larger Q^2 for which we want to predict the jet cross sections. For the structure function $F_2(x, Q^2)$ and $x F_3(x, Q^2)$ it has been shown from the analysis of recent measurements in high energy neutrino, electron and muon scattering that the Q^2 dependence is consistent with the expectations from QCD [14] . To have analytic expressions we employ a parametrization introduced by Buras and Gaemers [15] :

$$x(u-\bar{u}+d-\bar{d}) = \frac{3}{B(\eta_1(s),\, 1+\eta_2(s))}\, x^{\eta_1(s)}(1-x)^{\eta_2(s)}$$

$$x(d-\bar{d}) = \frac{1}{B(\eta_3(s),\, 1+\eta_4(s))}\, x^{\eta_3(s)}(1-x)^{\eta_4(s)} \qquad (2.18)$$

$$x\bar{s} = x\bar{u} = x\bar{d} = x\bar{s} = A(s)(1-x)^{\eta(s)}, \quad xg = A_g(s)(1-x)^{\eta_g(s)}$$

The functions u, $\bar{u}$, d, $\bar{d}$, s, $\bar{s}$ and g depend on x and Q^2. The Q^2 dependence is via

$$s = \ln \frac{\ln Q^2/\Lambda^2}{\ln Q_0^2/\Lambda^2} \qquad (2.19)$$

u, d and s are the densities of up, down and strange quarks in the proton. g is the gluon density. The parameters η_1, η_2, η_3, η_4, η , η_g, A and A_g at $Q^2 = Q_0^2 = 4\ \mathrm{GeV}^2$ were taken from a recent analysis of deep inelastic lepton scattering data (νN, $\bar{\nu}$N, ep, μp etc.) performed by Glück and Reya [16] . They obtained the following values:

$$\eta_1 = 0.624,\ \eta_2 = 2.657,\ \eta_3 = 0.773,\ \eta_4 = 3.7$$
$$\eta = 7 \quad ,\quad A = 0.17\ ,\ \eta_g = 5 \quad ,\ A_g = 2.6 \qquad (2.20)$$

The s-depende of these parameters is obtained by calculating the second and

third moment of the expressions (2.18) and comparing it with the well-known QCD formulas in the leading logarithm approximation. This way the s-dependence of the functions $\eta_1(s)$, $\eta_2(s)$ etc. which appear in (2.18) are fully determined if Λ is fixed. We assumed as in the Glück and Reya analysis: $\Lambda = 0.5$ GeV. This specifies the structure functions fa (x, Q^2) (a = u, d, s, $\bar{u}$, $\bar{d}$, $\bar{s}$, g) which enter in (2.5) and (2.10). The charm and anticharm content in the nucleon was neglected since it is really small [16] .

For the purpose of a rough comparison we have approximated the non-perturbative T distribution originating from (2.14) by [6] :

$$(\sigma_u^0)^{-1}\frac{d\sigma_u^0}{dT} = \frac{2(1-T)}{(\Delta T)^2}\, e^{-(1-T)^2/(\Delta T)^2} \qquad (2.21)$$

This gaussian form is motivated by the p_T distribution of the particles in a jet which is generally assumed to be of the form $e^{-bp_T^2}$. The factor (1-T) is for the fact that massive particles cannot be produced collinearly. The width parameter ΔT has been determined from a recent ν-nucleon scattering experiment at W = 10 GeV [17] . For the higher W-values the ΔT was scaled down with the factor $\langle n\rangle/W$, where $\langle n\rangle = 1 + 1.92\ \ln W^2$ is the multiplicity, which gives $\Delta T = 0.143$ for W = 10 GeV.

First we present some results for ep scattering based on the formulas (2.11), (2.12) and (2.13) with the structure functions described above. The angle which determines the azimuthal angle of the hadron plane is assumed to be fixed by choosing the vector p_1 in Fig. 2 to be the thrust axis, i. e. the momentum direction of the most energetic jet, in case a three-jet analysis is made. If this analysis is not made, it is of some advantage that one vector, the thrust direction, is sufficient to specify φ . Of course this is possible only if the lepton plane is already uniquely defined by the ingoing and outgoing lepton momenta (this would not be possible for $e^- \to \nu$ reactions). Then for various values of W^2 and Q^2 the resulting distributions $\frac{d\sigma_u}{dT}$, $\frac{d\sigma_L}{dT} = 2\frac{d\sigma_T}{dT}$ and $\frac{d\sigma_I}{dT}$, as a function of thrust T, always normalized with σ_u^0 , together with the non-perturbative distributions $(\frac{d\sigma_u}{dT})_{NP}$ and $(\frac{d\sigma_L}{dT})_{NP} = 2\,(\frac{d\sigma_T}{dT})_{NP}$ based on (2.14) and (2.21) are shown in Fig. 3a, b. With our choice of defining the hadron plane there is no contribution to $\frac{d\sigma_I}{dT}$ from two jets if the current and the target jet are not distinguished. The cross sections shown are calculated for W = 50 GeV, $x_B = \frac{1}{4}$ and $x_B = \frac{1}{2}$ (Fig. 3a) and W = 100 GeV with the same

x_B values (Fig. 3b). It is clear that W = 100 GeV is much more suitable to observe genuine three-jet effects than W = 50 GeV since in the former case the non-perturbative distribution is much narrower. For both W's the non-perturbative term of $\frac{d\sigma_L}{dT}$ is completely insignificant. Concerning the magnitude of $\frac{d\sigma_L}{dT}$ coming from three jets we observe little change in the interval $2/3 \lesssim T \lesssim 0.8$ if we change x_B from 1/4 to 1/2, but $\frac{d\sigma_L}{dT}$ becomes larger towards T = 1 for $x_B = \frac{1}{2}$. $\frac{d\sigma_I}{dT}$ decreases less steeply with decreasing thrust for $x_B = \frac{1}{2}$. Furthermore $\frac{d\sigma_U}{dT}$ is also larger for $x_B = \frac{1}{2}$ than for $x_B = \frac{1}{4}$. Thus for fixed W such kinematic conditions which result in larger values for x_B are more suitable to determine $\frac{d\sigma_U}{dT}$ and $\frac{d\sigma_I}{dT}$ in the interesting thrust region $2/3 \lesssim T \lesssim 0.9$. For a determination of $\frac{d\sigma_L}{dT}$ it may be better to choose smaller x_B because then the ratio $d\sigma_L / d\sigma_U$ is larger in the interval $0.8 \lesssim T \lesssim 0.9$.

We studied also the influence of the Q^2 dependence of the structure functions. For W = 2Q = 50 GeV and W = Q = 50 GeV we present the normalized $d\sigma_U/dT$, $d\sigma_L/dT$ and $d\sigma_I/dT$ with the structure functions (2.18) and with parameters (2.20) as deduced from measurements at $Q^2 = 4\ GeV^2$ in Fig. 4 and compare to the distributions of Fig. 3a which were computed with Q^2 dependent structure functions. As to be expected the cross sections are smaller for Q^2 dependent structure functions. In particular $d\sigma_L/dT$ is roughly a factor up to four smaller whereas $d\sigma_U/dT$ and $d\sigma_I/dT$ are decreased only by up to a factor two. For $x_B = \frac{1}{2}$ the difference is less dramatic. From this comparison we conclude that it is more realistic to use structure functions with scale breaking effects included.

The three-jet contribution to $d\sigma_U/dT$ is singular for $T \to 1$. $d\sigma_I/dT$ is somewhat less singular whereas $d\sigma_L/dT$ is finite for $T = 1$. The behaviour of these cross sections for $T \to 1$ is similar to the corresponding cross section in $e^+e^- \to qqg$ [13] and has its origin in the infrared problem of perturbative QCD. This infrared problem is very similar to the one already studied in QED. When computing cross sections the masslessness of gluons gives rise to divergences. One of the divergences comes from the emission of soft gluons by a quark. Infinities of this kind are cancelled order by order against the virtual corrections if the bremsstrahlung contributions are integrated over the gluon energy up to some cut-off energy ϵ.

Similarly, the second kind of infinity, the mass or collinear singularity, is cancelled against the virtual corrections by integrating the bremsstrahlung terms up to some angular cut δ [F3]. These terms together with the zero-order

terms define the two-jet contribution which is approximated by (2.21). Then the three-jet cross section comes only from the angular region $\theta \geq \delta$ and gluon energy region $E_g \geq \epsilon$. Instead with the cut-off parameters (ϵ, δ) we shall define the three-jet cross section as the cross section in the thrust region $T \leq T_0$. Reasonable values of T_0 are around $T_0 = 0.95$. These are the thrust values where $d\sigma_U/dT$ integrated from T = 2/3 up to $T = T_0$ is about 10 % of σ_U^0. If we compare this with the three-jet contribution in e^+e^- annihilation [3,19] using the same cut-off $T_0 = 0.95$ we see that the three-jet configuration in deep inelastic ep scattering occurs by roughly a factor two less frequent than in e^+e^- annihilation. The dependence of the 3-jet fraction f, which we define as

$$f = \frac{1}{\sigma_U^0} \int_{2/3}^{T_0} dT \frac{d\sigma_U}{dT} \qquad (2.22)$$

on the cut-off T_0 is shown in Fig. 5 for $x_B = \frac{1}{2}$ and W = 50, 100 and 200 GeV. We notice that for fixed T_0 the 3-jet fraction decreases with increasing W. Since with increasing W the cut-off T_0 should also be increased the 3-jet fraction increases with increasing W. For fixed T_0 and fixed W the fraction f decreases with decreasing x_B.

The interference cross section $d\sigma_I/dT$ is reduced by cancellation of contribution coming from different regions of integration because the orientation of the hadron plane was assumed to be determined by the thrust axis. This does not happen, if we define the orientation of the hadron plane always with the quark momentum direction. In this case, of course, one must be able to distinguish quark jets from gluon jets, which, at high energies, might be possible on the basis of higher multiplicities expected for gluon jets [F4]. The results for $d\sigma_I/dT$ together with the other cross sections are exhibited in Fig. 6 (W = 50 GeV, $x_B = \frac{1}{2}$). We see that $d\sigma_I/dT$ is much larger now in the interesting region of low thrust values. The nonperturbative contribution to $d\sigma_I/dT$ (see (2.14)) which does not cancel anymore is negligible in this T region and therefore does not cause any problem.

Similar results were obtained for νp and $\bar{\nu} p$ scattering. The general decomposition of the νp scattering cross section is (instead of (2.7))

$$\frac{d\sigma}{dQ^2 dW^2 d\varphi dx_1 dx_2} = \Gamma_\nu \left\{ \frac{d\sigma_{u_\ell}}{dx_1 dx_2} + (1-y)^2 \frac{d\sigma_{u_r}}{dx_1 dx_2} \right.$$

$$+ 2(1-y) \frac{d\sigma_L}{dx_1 dx_2} + 2(1-y)\cos 2\varphi \frac{d\sigma_T}{dx_1 dx_2}$$

$$\left. - (1-y)^{1/2} \cos\varphi \left[\frac{d\sigma_{I_\ell}}{dx_1 dx_2} + (1-y) \frac{d\sigma_{I_r}}{dx_1 dx_2} \right] \right\} \qquad (2.23)$$

with (2.24)

$$\Gamma_\nu = \frac{G_F^2 W^2 Q^2}{2\pi^2 (W^2+Q^2)^2}$$

The total cross section is written as in (2.9) with Γ replaced by Γ_ν. For $\nu + p \to \mu^- + X$ the zeroth-order cross section is

$$\sigma_u^0 = q_a \frac{1}{W^2} f_a(x_B, Q^2) \qquad (2.25)$$

It is left-handed for scattering on quarks and right-handed for scattering on antiquarks. G_F is the Fermi coupling constant and the factor q_a is for the coupling between the charged current and the interacting quark with flavour a. Of course, (2.25) includes a sum over quark flavours depending on the target p, n or $N = \frac{1}{2}$ (p+n). Our results are for a proton target.

For $\bar\nu$p scattering the general decomposition of the cross section is the same as (2.23) with (2.24) except that the labels l (left) and r (right) have to be interchanged. For antineutrino scattering the cross section in zeroth order is again given by (2.25).

The results for the various cross sections are shown in Fig. 7a,b ($\nu + p \to \mu^- +$ jets) and in Fig. 8a,b ($\bar\nu + p \to \mu^+ +$ jets), both for W = 50, $x_B = \frac{1}{2}$ and $\frac{1}{4}$ and with Q^2 dependent structure functions. All cross sections are normalized by $\sigma_{u_\ell}^0$ so that we plotted $(\sigma_{u_\ell}^0)^{-1} d\sigma_{u_\ell}/dT$ etc. We see that the QCD corrections give terms which contribute to $d\sigma_{u_r}$ which in zeroth order has contributions only from the antiquark structure functions. $d\sigma_{u_r}$ decreases with increasing x_B. In the interference terms $d\sigma_{I_r}$ dominates over $d\sigma_{I_\ell}$. We notice that $d\sigma_{u_r}/dT$ is somewhat larger for $\bar\nu$p scattering compared to $d\sigma_{u_\ell}/dT$ for νp scattering

which is roughly equal to $d\sigma_u/dT$ for ep scattering. Therefore in $\bar\nu$p scattering more three-jet events than in νp and ep reactions should be produced.

3. The Fragmentation Model

In this section we describe the jet fragmentation which is applied in the next section to predict the distributions originating from the two- and three-jet production. The model is the well-known Field-Feynman quark fragmentation model [21] which is modified to allow also diquark, triquark, fourquark and gluon fragmentation. The Field-Feynman model has been described amply in the literature [22] . Therefore we shall repeat only the main points and then describe the details of the generation of the target jet and the gluon jet.

We start with the zeroth order QCD contribution which is identical to the naive quark-parton model (QPM). In the center-of-mass frame ($\vec{q} + \vec{p} = 0$) the QPM (see Fig. 1f) yields a final state of a forward going quark q (in the direction of $\vec{q}$) and a backward going diquark qq (in the direction of $\vec{p}$).

The primary quark q_i of flavour i originating from the ingoing proton with $W_0 = (E + p_\parallel)_i$, where $p_\parallel$ is measured along a given jet axis, generates in its colour field a quark-antiquark pair $q_j\bar{q}_j$. The quark q_i and the antiquark $\bar{q}_j$ form a primary meson $q_i\bar{q}_j$ with $E + p_\parallel$ fraction $z_1 = \frac{E_1 + p_{\parallel 1}}{W_0}$ leaving $W_1 = (1 - z)W_0$ to a remaining quark with flavour j. This step is iterated and a cascade of mesons is produced. Quark-antiquark pairs generated in the colour field may be either $u\bar{u}$, $d\bar{d}$ or $s\bar{s}$ with probabilities 2:2:1. Spin 0 or 1 is randomly assigned to each meson with probability 1:1. The variable z is in every step randomly distributed between 0 and 1 according to

$$f(z) = 1 - a + 3a(1 - z)^2 \tag{3.1}$$

Every quark or antiquark is supposed to have a transverse momentum p_T randomly generated according to

$$f_q(p_T)\, d^2p_T = \frac{1}{\pi\sigma^2}\, e^{-p_T^2/\sigma^2}\, d^2p_T \tag{3.2}$$

with the constraint that the total p_T of each generated pair be zero. The primary meson $q_i\bar{q}_j$ then has a transverse momentum

$$(p_T)_{q_i\bar{q}_j} = (p_T)_{q_i} + (p_T)_{\bar{q}_j}$$

which is also gaussian distributed with

$$g(p_T)\, d^2p_T = \frac{1}{2\pi\sigma^2}\, e^{-p_T^2/2\sigma^2}\, d^2p_T \tag{3.3}$$

with the average $\langle p_T^2 \rangle = 2\sigma^2$. For a and σ we have chosen a = 0.70 and σ = 0.3 GeV as in an earlier analysis of jet production in e^+e^- annihilation [3].

The decay of the diquark qq which is created after the ingoing proton emitted the parton quark is described analogously. In the first step the diquark qq produces a baryon (stable or resonance) and an antiquark jet. The antiquark jet is assumed to decay into mesons in the same way as the quark jet described above. In analogy to the treatment of mesons we take into account only the stable baryons and the lowest lying baryon resonances of spin 1/2 and 3/2, i.e. N, Λ, Σ, N (1470), Δ (1232), Λ (1405) and Σ (1385). Ξ and Ω^- are left out. The decays of unstable baryons is formulated in a similar way as the decay of unstable mesons [21, 22] . Decay channels and branching ratios are taken from ref. 23.

We consider now the first order QCD diagrams (Fig. 1b, c and d). Then we have three jets, the x_1, x_2 and x_3 jet with $x_i = 2p_{io}/W$ (i = 1,2,3) (see Fig. 1e). The weight for such an event is calculated from eq. (2.11, 2.13) for the three cross sections σ_U, σ_L and σ_I separately. The x_1 jet starts with the direction (ϑ, φ) where $\vartheta = \chi_1$ in the polar angle of p_1 with respect to $\vec{q} \parallel z$ axis and $\varphi = 0$. We have $\cos\chi_1 = -1 + \frac{2(1-x_2)}{x_1 x_3}$.

The x_2 jet starts from $\vartheta = \chi_2$ ($\cos\chi_2 = -1 + \frac{2(1-x_1)}{x_2 x_3}$ and $\varphi = \pi$.

Then the x_3 jet is in the direction $\vartheta = \pi$, $\varphi = 0$. For the parton diagrams in Fig. 1b and 1d the x_2-jet is a gluon. The gluon fragmentation is assumed to be the two-step process

$$g \rightarrow q\bar{q} \rightarrow \text{hadrons} \tag{3.4}$$

This is a convenient method to implement the hadronization process of the gluons in a Monte-Carlo approach, since there is no evidence yet for pure gluonic hadron states. The production of $q\bar{q}$ in (3.4) is similar to the $q\bar{q}$ pair creation in the Field-Feynman quark jet hadronization model. The step $g \rightarrow qq$ in (3.4) is described by a z-independent ($z = E_q/E_g$) primordial gluon fragmentation function

$f_g^q(z)$ = const. This differs from the splitting function $f_g^q(z) = z^2 + (1-z)^2$ [24] which was used recently in calculations of the process $e^+e^- \to qqg$ hadrons [3] . However, it has been found there that the exact shape of this function does not affect the final distributions severely [3] .

In case that the parton coming off the proton is a gluon, i.e. the parton diagram Fig. 1b is substituted by Fig. 1c in Fig. 1e, the x_3 jet is a triquark state. This triquark is assumed to decay into one of the baryons listed above plus a photon. In the case that the parton which absorbs the virtual boson (γ or $W^{\pm}$) is an antiquark (Fig. 1d) the x_3 jet is a four quark state. This, then, decays into a baryon and a quark jet which transforms into mesons as in the original Field-Feynman model. Thus in all cases, whether zeroth or first order QCD contributions, the cascades originate from the fragmentation of quarks or antiquarks.

In order to test at least parts of our fragmentation model we calculated the thrust (T) and spherocity (S) distributions for the zeroth order contribution (Fig. 1f) and compared them with recent experimental distributions at rather low $W \lesssim 10$ GeV [25, 26] . At these center-of-mass energies the T and S distributions are dominated by the two-jet contributions and the three-jet terms can safely be neglected (the influence of the three-jet contributions at these low W is discussed in the next section). Fig. 9a shows the T distribution $\frac{1}{\sigma}\frac{d\sigma}{dT}$ at W = 10 GeV compared to the data from BEBC (ν Ne-H_2) [25] and Fig. 9b the spherocity distribution $\frac{1}{\sigma}\frac{d\sigma}{dS}$ compared to data coming from the same experiment. In Fig. 10a, b we display the normalized sphericity distributions $\frac{1}{\sigma}\frac{d}{d\hat{S}}$ for $\bar{\nu}$p reactions with W = 6.6 GeV and W = 10.5 GeV respectively. They are compared with the measured distributions at the same energies [26] . Actually the experimental points in Fig. 10b present data for $\bar{\nu}$p plus νp reactions. The theoretical curves for νp and $\bar{\nu}$p scattering differ, however, very little. In total we conclude that the theoretical curves agree quite well with the measured points. Perhaps at W = 10 GeV the tails of the distributions at large S, $\hat{S}$ and at small T are somewhat flatter experimentally. If we include a three-jet contribution with a cut - off at $T_0 = 0.95$ as described in more detail in the next section we get the dashed curves in Fig. 9a, b and 10a, b. Indeed, the three-jet terms flatten the distributions and the agreement with the experimental data improves. But, of course, one needs higher energies W, to see clearly the effect of the extra three-jet contribution.

4. Results with Fragmentation

In this section we present results for several distributions with fragmentation of quark and gluons into hadrons taken into account which show explicitly the contribution of the three-jet terms. It is clear that many distributions in one or two jet variables can be looked at which are sensitive to the higher order QCD contributions. Here we exhibit the thrust distributions $\frac{d\sigma_u}{dT}$, $\frac{d\sigma_I}{dT}$ and $\frac{d\sigma_I}{dT}$ and the distribution of σ_u in the variables $p_{T\,in}^2$ and $p_{T\,out}^2$.

The momentum components $p_{T\,in}$ and $p_{T\,out}$ were calculated with respect to eigenvectors n_1, n_2 and n_3 of the second rank tensor

$$M_{\alpha\beta} = \sum_{j=1}^{N} p_{j\alpha}\, p_{j\beta} \qquad (\alpha,\beta = x,y,z) \tag{4.1}$$

where the sum over j runs over the N particles of the event. $\hat{n}_1$, $\hat{n}_2$ and $\hat{n}_3$ are the unit eigenvectors of this tensor with eigenvalues Q_1, Q_2 and Q_3 in the order $Q_1 \leq Q_2 \leq Q_3$. The principal jet axis is along the $\hat{n}_3$ direction and $\hat{n}_2$ - $\hat{n}_3$ define the event plane. $\hat{n}_1$ is the direction in which the sum of the squared hadron momentum components is minimized. Then

$$p_{T\,in}^2 = \frac{1}{N}\sum_{j=1}^{N} (\vec{p}_j \hat{n}_2)^2 \tag{4.2}$$

and

$$p_{T\,out}^2 = \frac{1}{N}\sum_{j=1}^{N} (\vec{p}_j \hat{n}_1)^2 \tag{4.3}$$

The $p_{T\,out}$ - distribution should show only the effect of the jet broadening caused by the fragmentation of quarks and gluons whereas the $p_{T\,in}$ distribution should exhibit the existence of the third jet coming from the gluon emission or absorption.

These three distributions, in thrust T, in $p_{T\,in}^2$ and $p_{T\,out}^2$ are shown in Fig. 11, 12, 13 and 14. In Fig. 11 and 12 it is for ep scattering and for W = Q = 50 GeV (Fig. 11) and W = Q = 100 GeV (Fig. 12). Fig. 13 shows the same distribution for νp scattering. Here only the dominant cross sections σ_{u_ℓ} and σ_{I_r} are plotted. Fig. 14 is for $\bar{\nu}$p scattering with σ_{u_r} and σ_{I_ℓ} . For comparison also the two-jet distributions $(\frac{d\sigma_u}{dT})_{2\ jets}$ are plotted in Fig. 11a, 12a, 13a and 14a. To separate two jets from three jets we introduced

in the three-jet fragmentation the cut-off at $T_o = 0.95$ as was explained in section 2. For W = 100 GeV this cut-off was increased to $T_o = 0.975$. This way the three-jet contribution smoothly connects with the two-jet contribution. Actually this is not really important since for this large thrust value the distribution is modified by higher order perturbative terms. The normalization of all curves is such that the integral over $\frac{d\sigma_u}{dT}$ (or $\frac{d\sigma_{ue}}{dT}$ for νp, or $\frac{d\sigma_{\bar{u}e}}{dT}$ for $\bar{\nu} p$) which includes three- and two-jet contributions separated by $T = T_o$ is normalized to one. Then the relative normalization of $\frac{d\sigma_L}{dT}$ and $\frac{d\sigma_I}{dT}$ is given by the formulas in section 2.

The definition of the azimuth angle φ is still based on the quark, antiquark or gluon momenta as in section 2. This means we have not determined the distribution from the actual events by fitting them to the distribution (2.7). This may cause some small error concerning our predictions of σ_I and σ_T which should decrease with increasing W. Similarly a finite target p_T, which was neglected here, also has some effect on the φ distribition. Of course, with increasing Q^2 the effect of finite target p_T should go away also. But the initial target p_T has no influence on the thrust, sphericity etc. distributions since they are calculated totally from the properties of the final state irrespective of the momentum of the incoming parton.

Concerning the relative normalization of σ_u, σ_L and σ_I our results are accurate only for the rather large Q^2 considered in this paper. For low Q^2 experiments the effects of finite target p_T should be taken into account.

By comparing the curves in Fig. 11a with Fig. 3a we see the effect of the smearing caused by the fragmentation. First we notice that the two-jet distribution is somewhat narrower than the estimates based on eq. (2.21). Second the influence of the smearing in the three-jet region is not very dramatic except for smaller T values, where the hadronization produces a tail beyond the kinematic limit T = 2/3. The conclusions are similar if one compares Fig. 13a with the curves in Fig. 7a and Fig. 14a with Fig. 8a respectively. For W = 50 GeV the effect of three jets is clearly visible in the thrust distribution.

For $\bar{\nu}p$ scattering we notice in Fig. 14a some small minimum in the T-distribution near T = 0.9. This is caused by the introduction of the cut-off at T = 0.95 in the three-jet generation. In this T region the higher-order correction come in so that our prediction in this region will be modified. Therefore for testing the underlying theory one has to restrict the comparison with experimental data to smaller T values anyway. Such a dip does not occur in the ep

and νp distributions because in these cases the three-jet part is smaller. In table 1 we give the percentage of two-jet and three-jet contribution for the various cases (W = 50 GeV with $T_o = 0.95$ and W = 100 GeV with $T_o = 0.975$). We see that with the same T_o the three-jet cross section in $\bar{\nu} p$ is almost twice the three-jet cross section in ep and νp scattering.

5. Summary

In this paper we made realistic predictions for jet production in deep inelastic lepton-proton scattering. We calculated various distributions in particular in thrust, $p_{T\ in}^2$ and $p_{T\ out}^2$. The fragmentation model was tested by comparing with low energy neutrino and antineutrino scattering data where the nonperturbative two-jet contribution dominates. These data are also consistent with our QCD model which correctly predicts the distribution at smaller T and larger sphero-city or sphericity.

Not all aspects of this three-jet production model have been considered in this paper. For example, in case the target jet can be separated, as one expects in high energy ep collisions with HERA [7] one is left with only two jets, quark and gluon or quark and antiquark. Since the $q\bar{q}$ contribution is less frequent deep inelastic ep scattering might offer a better possibility to study the properties of the gluon jet as in e^+e^- annihilation where one is dealing always with three jets.

We have seen that the effect of final parton fragmentation is not very large as compared to e^+e^- annihilation [3] . We also found that the three-jet contribu-tion varies as a function of Q^2 for fixed W^2 and thrust cut-off T_o. This offers the possibility to study the QCD effects as a function of Q^2 without the effect of broadening the two-jet contribution as it occurs in e^+e^- annihilation if $Q^2 = E_{c.m.}^2$ is decreased.

Acknowledgement: We thank A. Ali and G. Schierholz for helpful discussions.

Table

Process	T_o	W [GeV]	Q [GeV]	$\sigma_{3\text{-Jet}}/(\sigma_{2\text{-Jet}}+\sigma_{3\text{-Jet}})$	$\langle 1-T\rangle$	$\langle\hat{s}\rangle$	$\langle p_{T\ out}^2\rangle$	$\langle p_{T\ in}^2\rangle$
ν p	0.95	50	50	0.20	0.055	0.035	0.031	0.100
$\bar{\nu}$ p	0.95	50	50	0.37	0.070	0.050	0.032	0.135
ep	0.95	50	25	0.11	0.050	0.026	0.030	0.080
ep	0.95	50	50	0.18	0.050	0.030	0.030	0.100
ep	0.975	100	100	0.33	0.036	0.018	0.034	0.186

References

1 J. Ellis, M.K. Gaillard and G.G. Ross, Nucl. Phys. B 111 (1976) 253,
E.G. Floratos, Il Nuovo Cimento 43A (1978), 241,
T.A. DeGrand, Y.J. Ng and S.-H.H. Tye, Phys. Rev. D16 (1977) 3251

2 R. Brandelik et al., Phys. Lett. 86B (1979) 243
Ch. Berger et al., Phys. Lett. 86B (1979) 418
D.P. Barber et al., Phys. Rev. Lett. 43 (1979) 830
W. Bartel et al., Phys. Lett. 91B (1980) 142

3 A. Ali, E. Pietarinen, G. Kramer and J. Willrodt
Phys. Lett. 93B (1980) 155

4 H. Georgi and J. Sheiman, Phys. Rev. D20 (1979) 111
A. Méndez and T. Weiler, Phys. Lett. 83B (1979) 221
J. Ranft and G. Ranft, Phys. Lett. 82B (1979) 129
P. Binétruy and G. Girardi, Nucl. Phys. B155 (1979) 150
Ch. Rumpf and G. Kramer, Phys. Lett. 89B (1980) 380

5 See also: G.C. Fox, T.-Y. Tse and S. Wolfram, Nucl. Phys. B165 (1980) 80

6 Ch. Rumpf and G. Kramer, see ref. 4

7 See part IV in the: Report of the Electron Proton Working Group of ECFA,
Study on the Proton-Electron Storage Ring Project HERA, ECFA 80/42
(17 March 1980) DESY HERA 80/01.

8 N. Schmitz, preprint MPI-PAE/Exp. EL.80 (1979)
and in Proceedings of the 1979 International Symposium on Lepton and
Photon Interactions at High Energies (to be published)

9 H. Georgi and H.D. Politzer, Phys. Rev. Lett. 40 (1978) 3

10 N.S. Craigie, G. Kramer and J.G. Körner, Nucl. Phys. B68 (1974) 509

11 R.P. Feynman, Photon-Hadron Interactions, Benjamin, Reading/Mass. 1972
R.N. Cahn, Phys. Lett. 78B (1978) 269

12 R.L. Kingsley, Phys. Rev. D10 (1974) 1580

13 A. de Rújula, J. Ellis, E.G. Floratos and M.K. Gaillard,
Nucl. Phys. B138 (1978) 387

14 H.L. Anderson et al., Phys. Rev. Lett. 40 (1978) 1061
P.C. Bosetti et al., Nucl. Phys. B142 (1978) 1
J.G.H. de Groot et al., Z. Physik C1 (1979) 193, Phys. Lett. 82B (1979)
292, 450

15 A. Buras and K.J.F. Gaemers, Nucl. Phys. B132 (1978) 249

16 M. Glück and E. Reya, DESY report 79/13 and Nucl. Phys. B156 (1979) 456

17 K.W.J. Barnham et al., Phys. Lett. 85B (1979) 300

18 H.D. Politzer, Nucl. Phys. B129 (1977) 301, Phys. Lett. 70B (1977) 430
D. Amati, R. Petronzio and G. Veneziano, Nucl. Phys. B140 (1978) 54
P.M. Stevenson, Nucl. Phys. B150 (1979) 357

19 G. Kramer, Lectures at IX International Summer Institute on Theoretical
Physics, Kaiserslautern, August 1979 (to be published)

20 F. Hayot and A. Morel, Z.Physik C3 (1980) 239

21 R.D. Field and R.P. Feynman, Nucl. Phys. B136 (1978) 1

22 T. Sjöstrand, Lund report LU TP 79-8 and references therein.

23 Particle Data Group, Phys. Lett. 75B (1978) 1

24 G. Altarelli and G. Parisi, Nucl. Phys. B126 (1977) 298

25 K.W.J. Barnham et al., Phys. Lett. 85B (1979) 300

26 M. Derrick et al., Phys. Lett. 88B (1979) 177.

Footnotes:

F1 For a review of these data see ref. 8.

F2 For results with off-shell quarks see ref. 12.

F3 Of course, unlike the e^+e^- - annihilation case the divergences do not all cancel. Using the Lee-Nauenberg - Kinoshita theorem one finds that the remaining divergences can be factorized into the quark distribution function in the sense of Politzer [18] and therefore are taken into account in the Q^2 dependent structure functions.

F4 For another possibility to trigger on gluon jets see ref. 20.

Figure Captions

Fig. 1: (a) Zeroth order diagram for lepton-parton scattering. (b, c, d) First order parton diagram for lepton-parton scattering. (e) Kinematic diagram for three-jet production, (f) for two-jet production in lepton-proton scattering.

Fig. 2: Kinematics of lepton-hadron scattering in the hadronic final state rest frame showing the azimuthal angle φ.

Fig. 3: Partial cross sections U: $d\sigma_U/dT$, L: $d\sigma_L/dT$, I: $d\sigma_I/dT$ and T: $d\sigma_T/dT = \frac{1}{2} d\sigma_L/dT$ for jet production in ep scattering. The dashed curves are the nonperturbative cross sections. For (a) W = 50 GeV, Q = 25 GeV, (b) W = 50 GeV, Q = 50 GeV, (c) W = 100 GeV, Q = 50 GeV and (d) W = 100 GeV, Q = 100 GeV.

Fig. 4: Same cross sections as Fig. 3 with Q^2 independent structure functions for (a) W = 50 GeV, Q = 25 GeV and (b) W = 50 GeV, Q = 50 GeV.

Fig. 5: Integrated three-jet cross section as a function of thrust cut-off T_0 for W = Q = 50, 100 and 200 GeV.

Fig. 6: Same cross sections as Fig. 3 for hadron plane defined with quark momentum and W = 2Q = 50 GeV.

Fig. 7: Partial cross sections U_μ: $d\sigma_{U_\mu}/dT$, U_e: $d\sigma_{U_e}/dT$, L: $d\sigma_L/dT$, T: $d\sigma_T/dT$, I_μ: $d\sigma_{I_\mu}/dT$ and I_e: $d\sigma_{I_e}/dT$ for jet production in νp scattering. For (a) W = Q = 50 GeV, (b) W = 2Q = 50 GeV.

Fig. 8: Same cross sections as in Fig. 7 for $\bar{\nu}$p scattering and (a) W = Q = 50 GeV, (b) W = 2Q = 50 GeV.

Fig. 9: Comparison of neutrino scattering data from BEBC [25] at W = Q = 10.5 GeV with two-jet and three-jet model (a) $\frac{1}{\sigma}\frac{d\sigma}{dT}$ and (b) $\frac{1}{\sigma}\frac{d\sigma}{dS}$. The full line is the two-jet model, the broken line the three-jet model.

Fig. 10: Comparison of sphericity distributions $\frac{1}{\sigma}\frac{d\sigma}{d\hat{S}}$ for anti-neutrino scattering predicted by two-jet and three-jet model with data of ref. 26. (a) is for W = Q = 6.6 GeV and (b) is for W = Q = 10.5 GeV. The full line is the two-jet model, the broken line the three-jet model.

Fig. 11: (a) Thrust distributions $d\sigma_U/dT\,(U)$, $d\sigma_L/dT = 2\,d\sigma_T/dT\,(L)$ and $d\sigma_I/dT$ (I) for ep scattering at W = Q = 50 GeV. $d\sigma_{U_{2\text{-jet}}}/dT\,(U_{2\text{-jet}})$ is the nonperturbative two-jet contribution; (b) $p_{T\ in}^2$ distribution of σ_U; (c) $p_{T\ out}^2$ distribution of σ_U for same parameters.

Fig. 12: (a), (b) and (c) as in Fig. 11 for W = Q = 100 GeV

Fig. 13: (a), (b) and (c) as in Fig. 11 for νp scattering and W = Q = 50 GeV. U stands for U_e, I for I_r.

Fig. 14: (a), (b) and (c) as in Fig. 11 for $\bar{\nu}$p scattering and W = Q = 50 GeV. U stands for U_r, I for I_e.

Table Caption:

Thrust cut-off T_0, relative three-jet contribution and averge values of 1-T, $\hat{S}$, $p_{T\ out}^2$ and $p_{T\ in}^2$ for νp, $\bar{\nu}$p and ep scattering for various W and Q values.

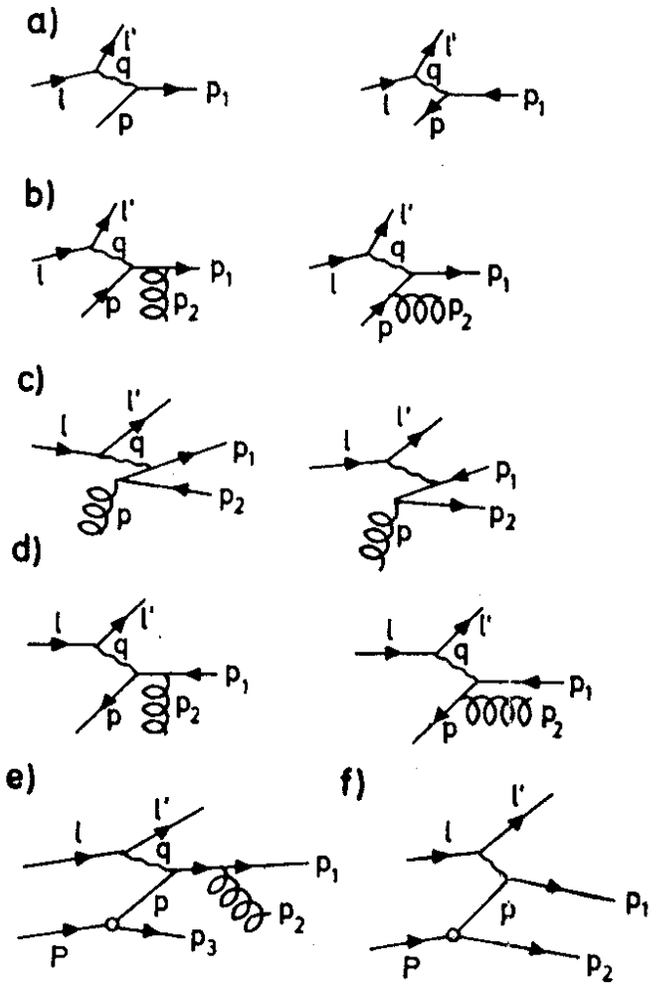

Fig 1

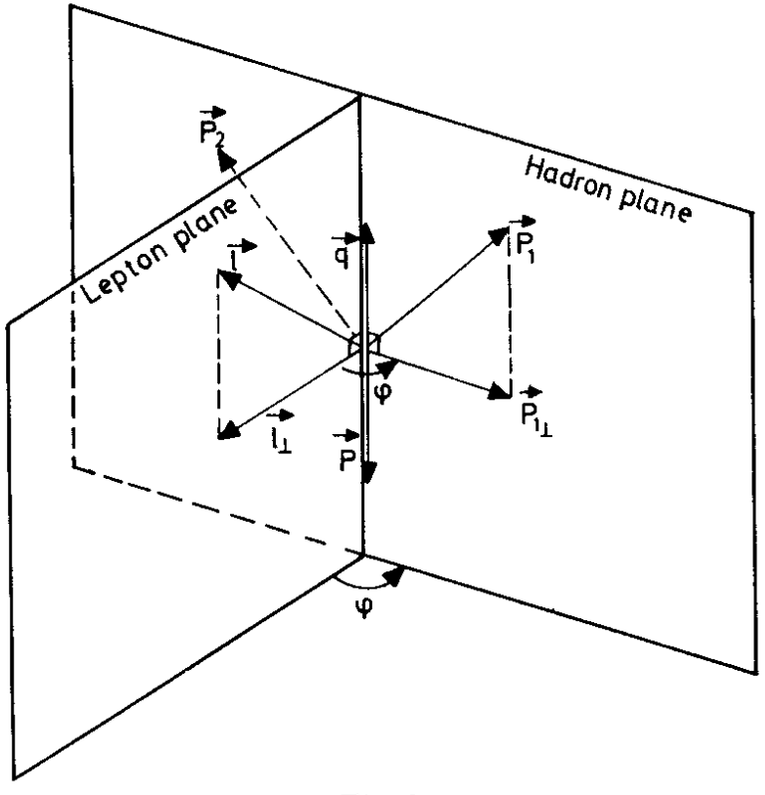
Lepton plane
Hadron plane
$\vec{P}_2$
$\vec{l}$
$\vec{q}$
$\vec{P}_1$
φ
$\vec{l}_\perp$
$\vec{P}$
$\vec{P}_{1\perp}$
φ

Fig.2

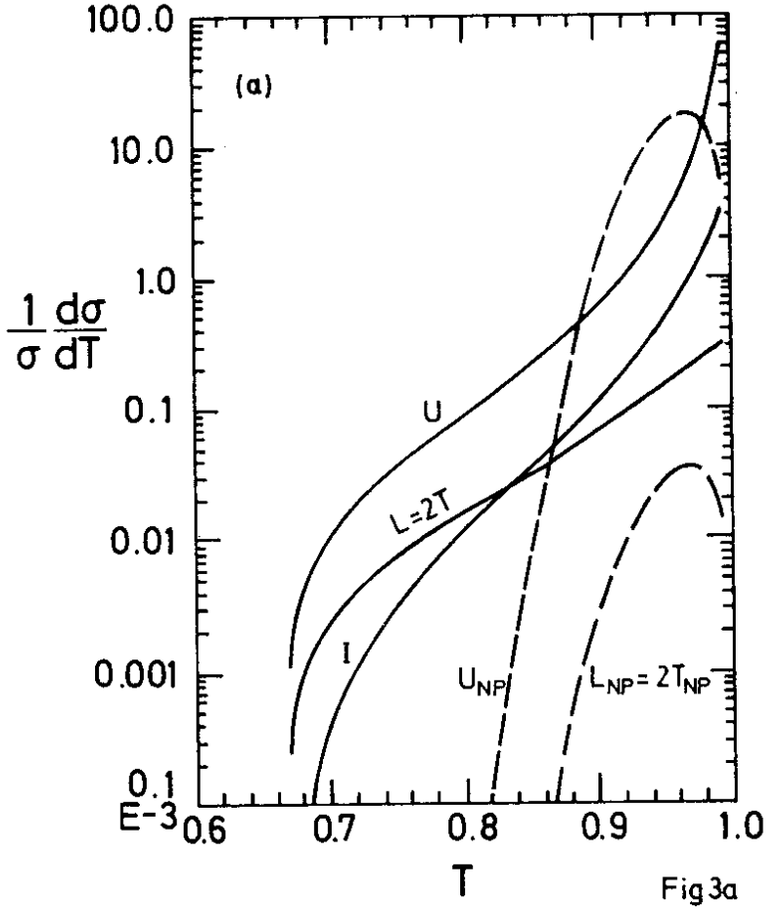
100.0
10.0
1.0
0.1
0.01
0.001
0.1
E-3
(a)
$\frac{1}{\sigma}\frac{d\sigma}{dT}$
U
L=2T
I
U_{NP}
$L_{NP}=2T_{NP}$
0.6
0.7
0.8
0.9
1.0
T

Fig 3a

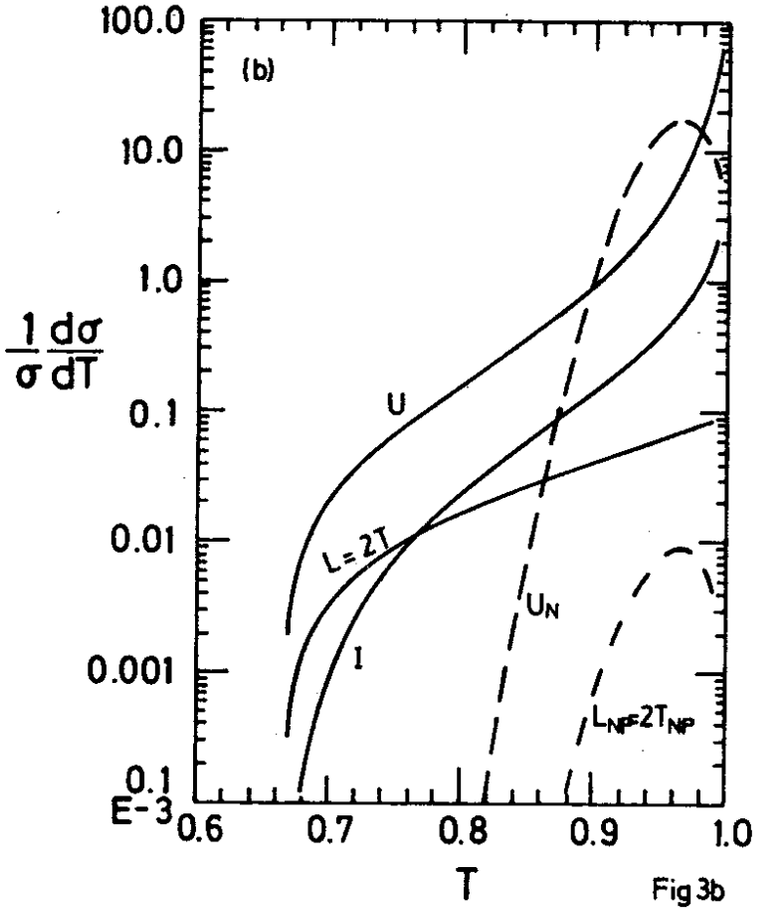
(b)
100.0
10.0
1.0
0.1
0.01
0.001
0.1
E-3
0.6
0.7
0.8
0.9
1.0
T
1 dσ / σ dT
U
L=2T
I
U_N
L_NP=2T_NP

Fig 3b

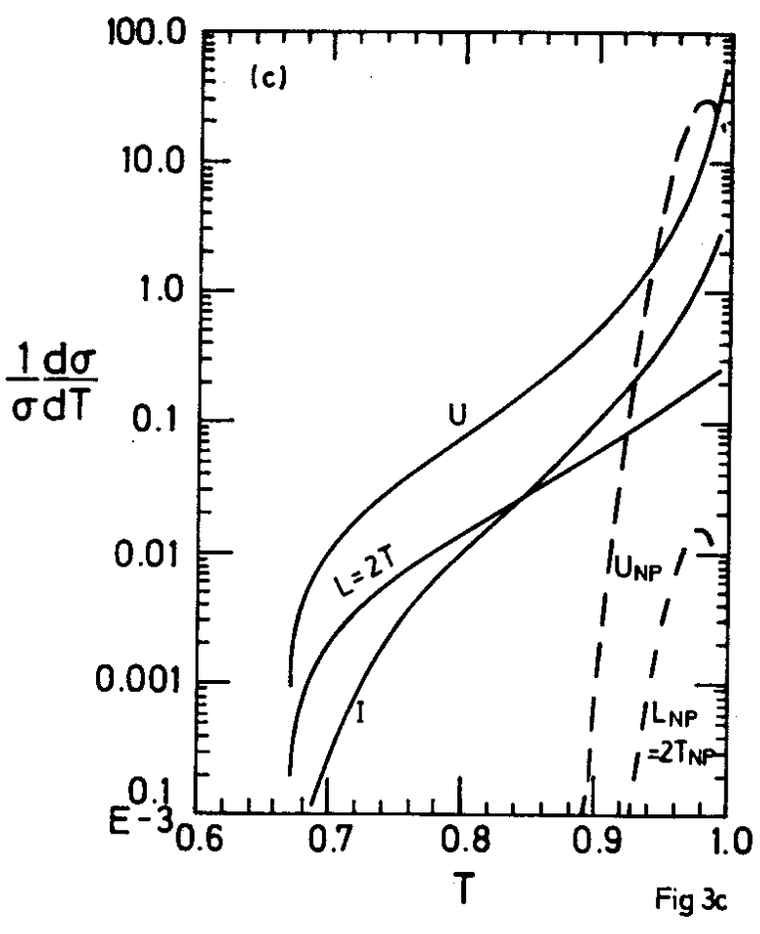
(c)
100.0
10.0
1.0
0.1
0.01
0.001
0.1
E-3
0.6
0.7
0.8
0.9
1.0
T
1 dσ / σ dT
U
L=2T
I
U_NP
L_NP
=2T_NP

Fig 3c

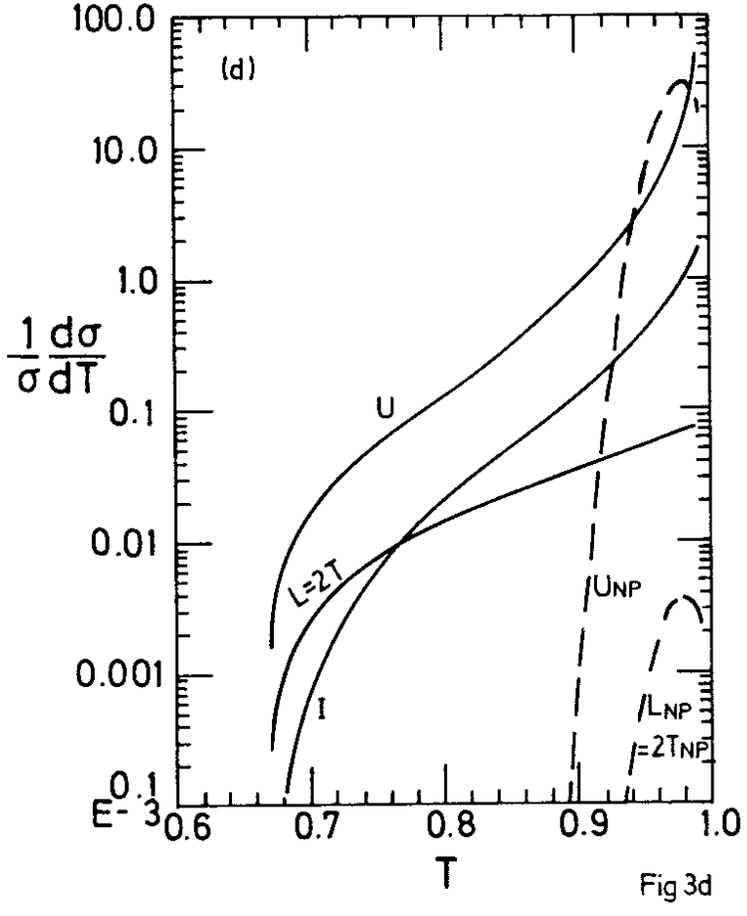
(d)
100.0
10.0
1.0
0.1
0.01
0.001
0.1
E-3
0.6
0.7
0.8
0.9
1.0
T
1/σ dσ/dT
U
L=2T
I
UNP
LNP
=2TNP

Fig 3d

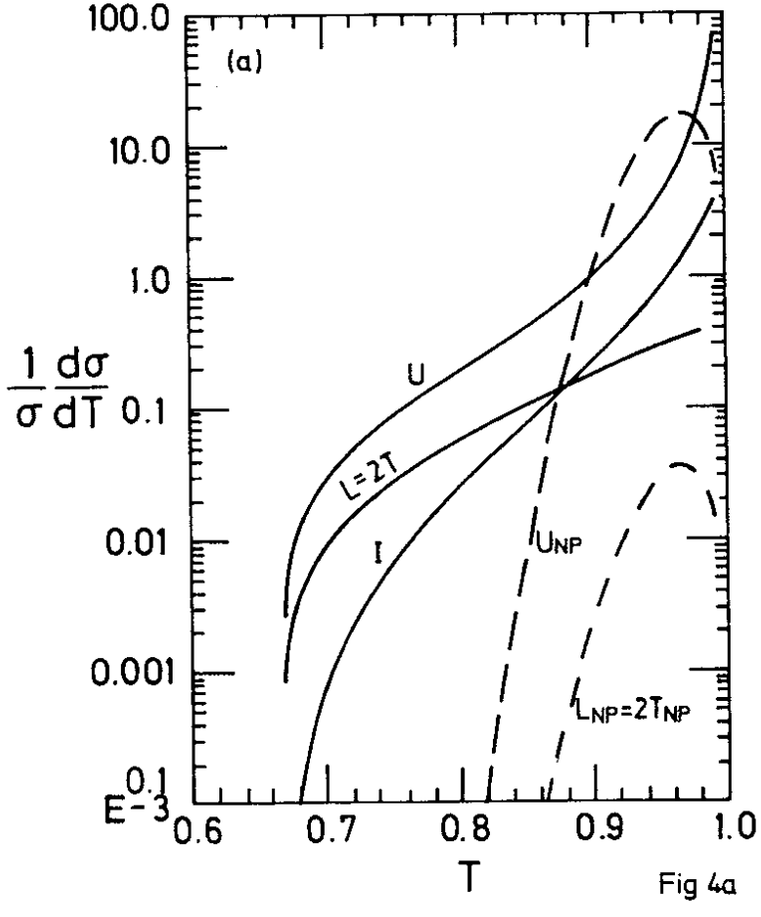
(a)
100.0
10.0
1.0
0.1
0.01
0.001
0.1
E-3
0.6
0.7
0.8
0.9
1.0
T
1/σ dσ/dT
U
L=2T
I
UNP
LNP=2TNP

Fig 4a

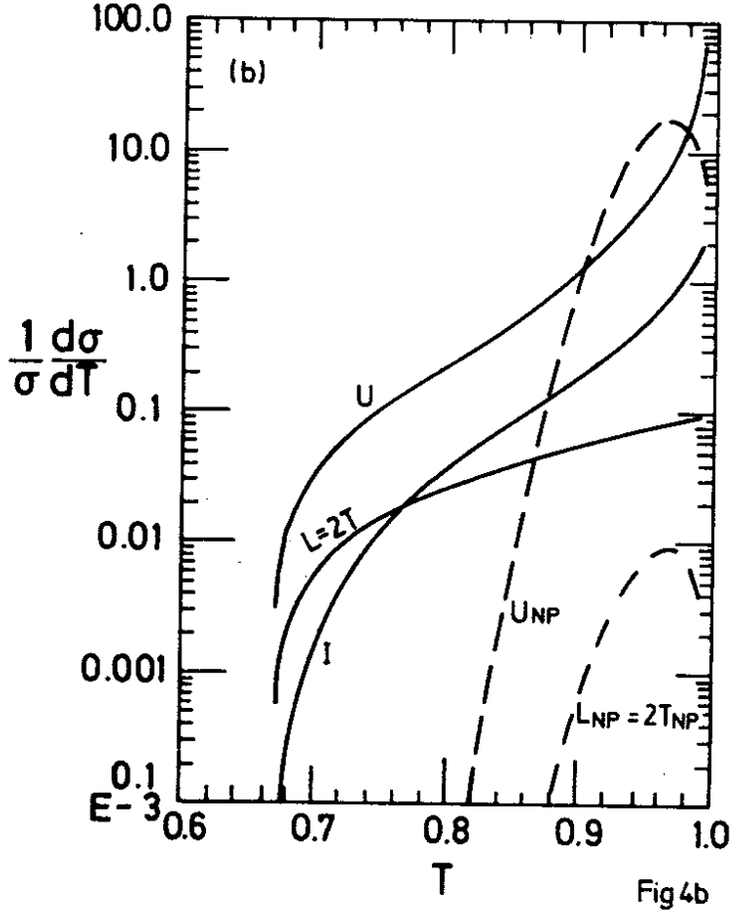
(b)
100.0
10.0
1.0
0.1
0.01
0.001
0.1
E^{-3}
$\frac{1}{\sigma}\frac{d\sigma}{dT}$
U
L=2T
I
U_{NP}
$L_{NP} = 2T_{NP}$
0.6
0.7
0.8
0.9
1.0
T

Fig 4b

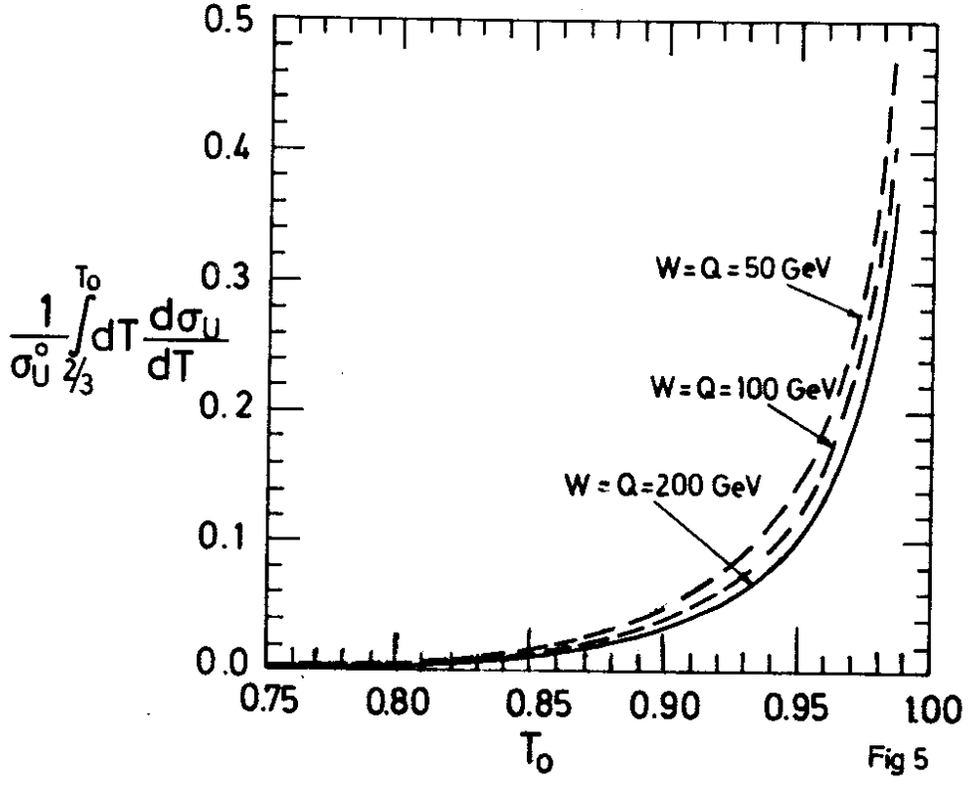
$\frac{1}{\sigma_U^0}\int_{2/3}^{T_0} dT \frac{d\sigma_U}{dT}$
0.5
0.4
0.3
0.2
0.1
0.0
W=Q=50 GeV
W=Q=100 GeV
W=Q=200 GeV
0.75
0.80
0.85
0.90
0.95
1.00
T_0

Fig 5

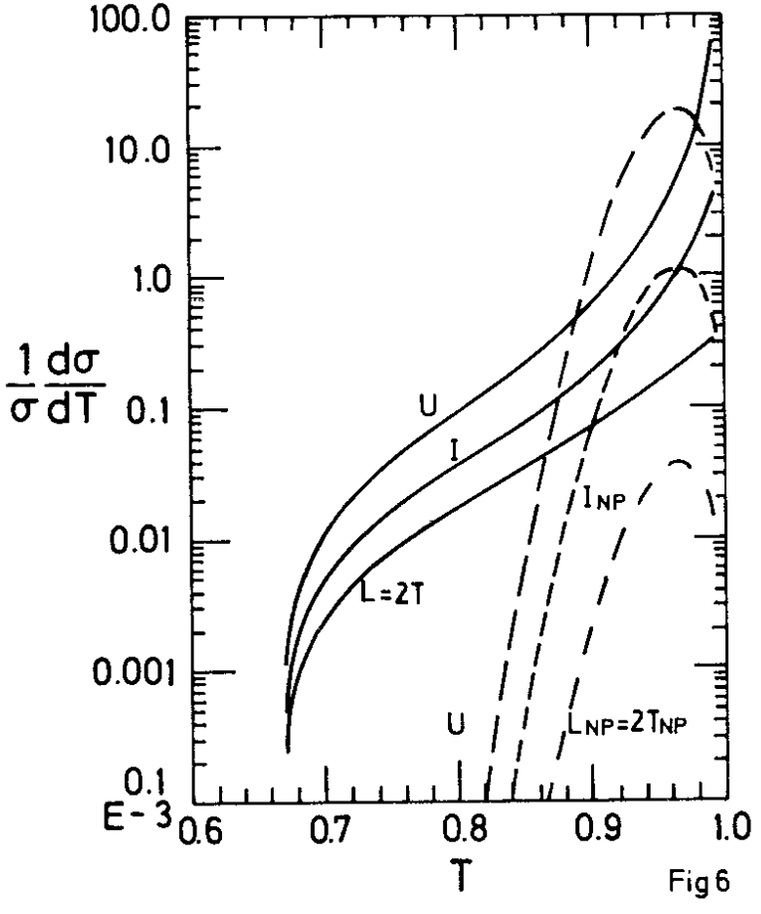
100.0
10.0
1.0
0.1
0.01
0.001
0.1
E-3
0.6
0.7
0.8
0.9
1.0
T
1/σ dσ/dT
U
I
L=2T
U
I_NP
L_NP=2T_NP

Fig 6

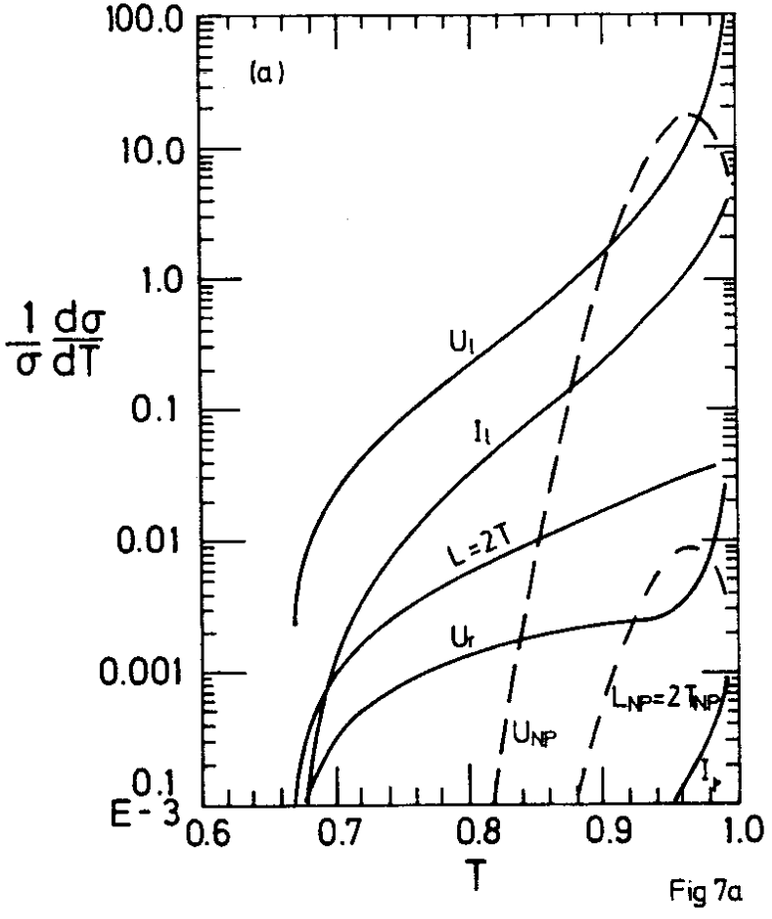
(a)
100.0
10.0
1.0
0.1
0.01
0.001
0.1
E-3
0.6
0.7
0.8
0.9
1.0
T
1/σ dσ/dT
U_l
I_l
L=2T
U_r
U_NP
L_NP=2T_NP
I_r

Fig 7a

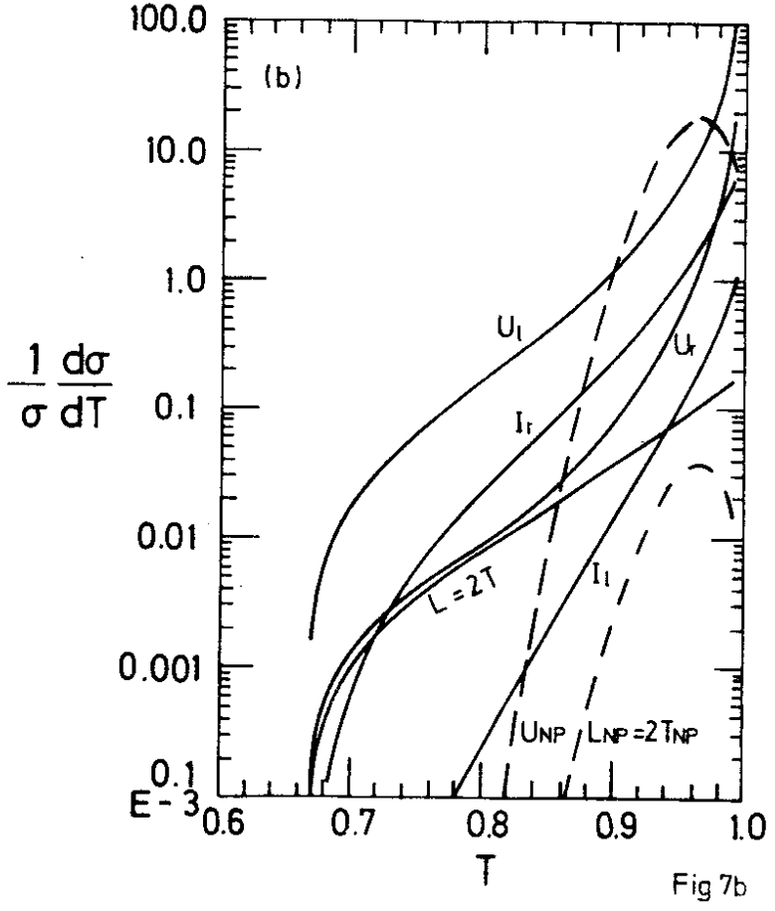
(b)
100.0
10.0
1.0
0.1
0.01
0.001
0.1
E-3
0.6
0.7
0.8
0.9
1.0
T
1 dσ / σ dT
U_l
I_r
U_r
L=2T
I_l
U_NP
L_NP=2T_NP

Fig 7b

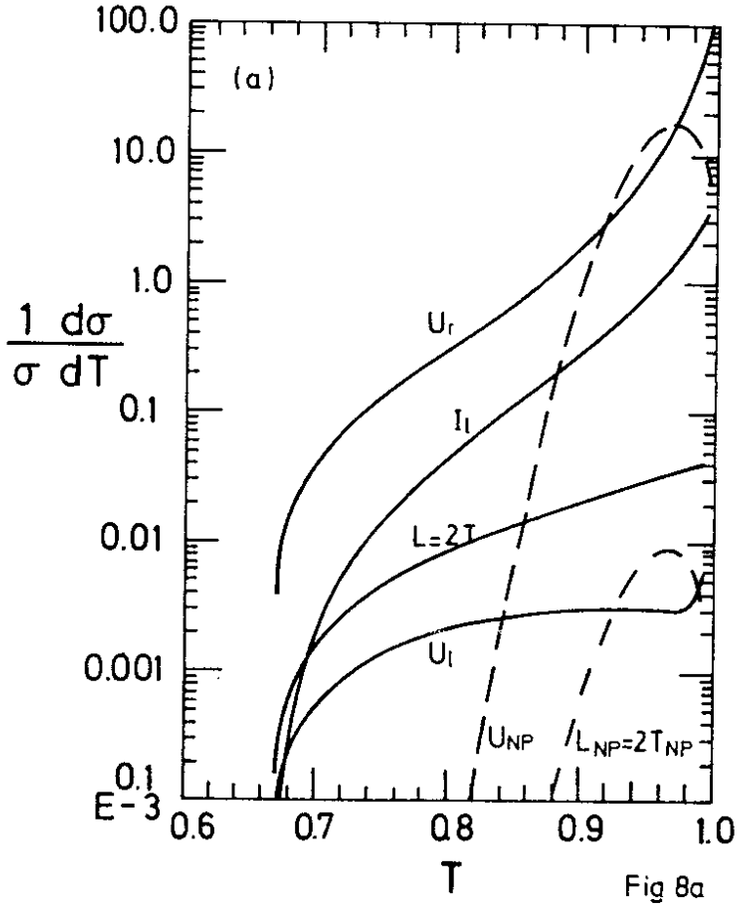
(a)
100.0
10.0
1.0
0.1
0.01
0.001
0.1
E-3
0.6
0.7
0.8
0.9
1.0
T
1 dσ / σ dT
U_r
I_l
L=2T
U_l
U_NP
L_NP=2T_NP

Fig 8a

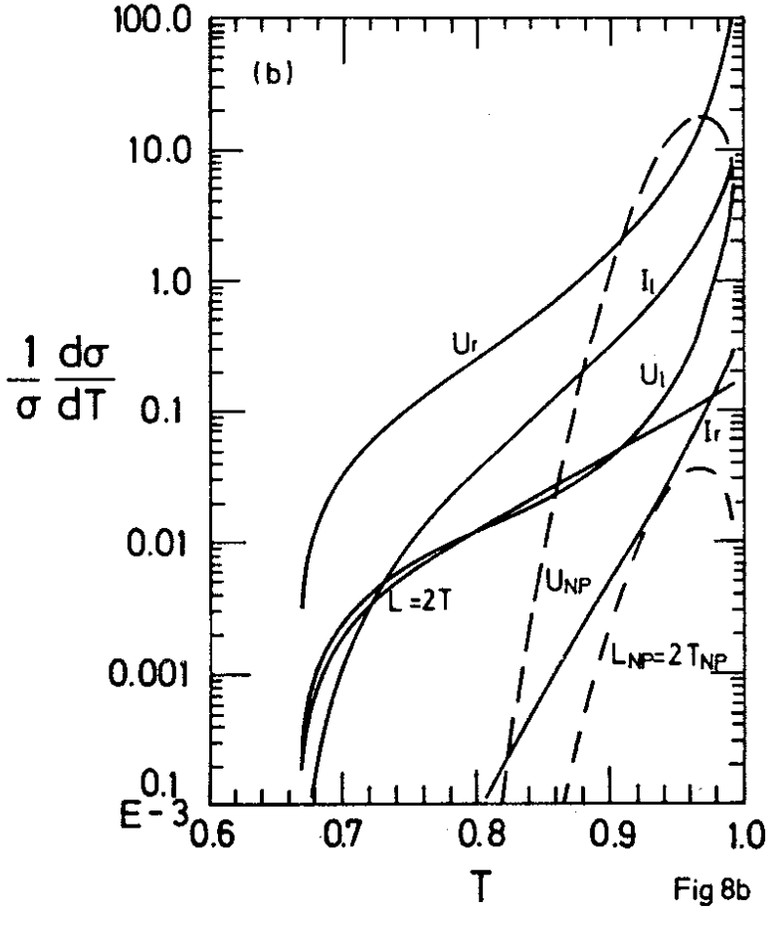
(b)
100.0
10.0
1.0
0.1
0.01
0.001
0.1
E-3
0.6
0.7
0.8
0.9
1.0
T
1/σ dσ/dT
Ur
Il
Ul
Ir
UNP
L=2T
LNP=2TNP

Fig 8b

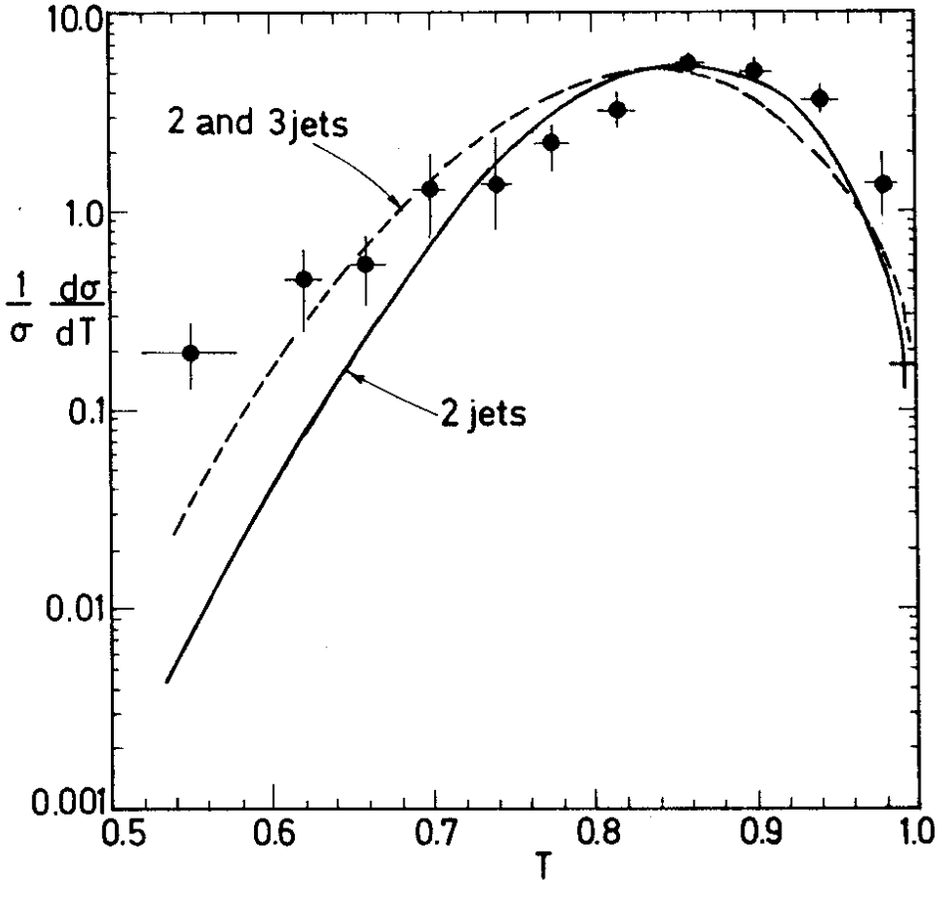
10.0
1.0
0.1
0.01
0.001
0.5
0.6
0.7
0.8
0.9
1.0
T
1/σ dσ/dT
2 and 3jets
2 jets

Fig.9a

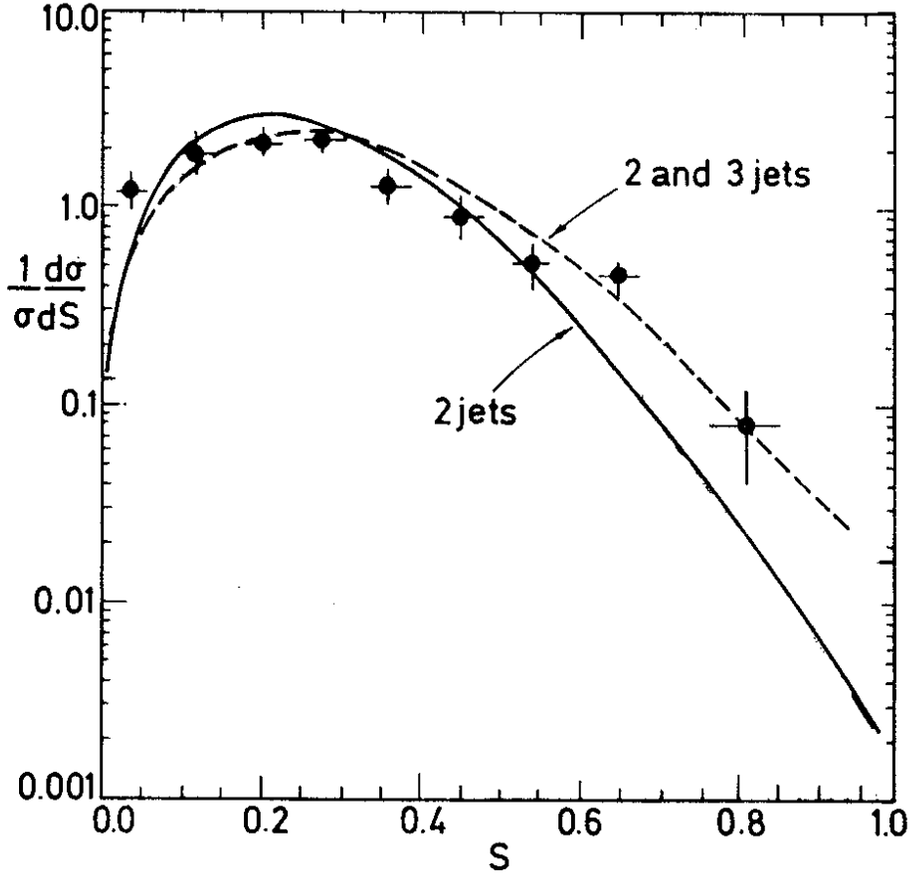

Fig.9b

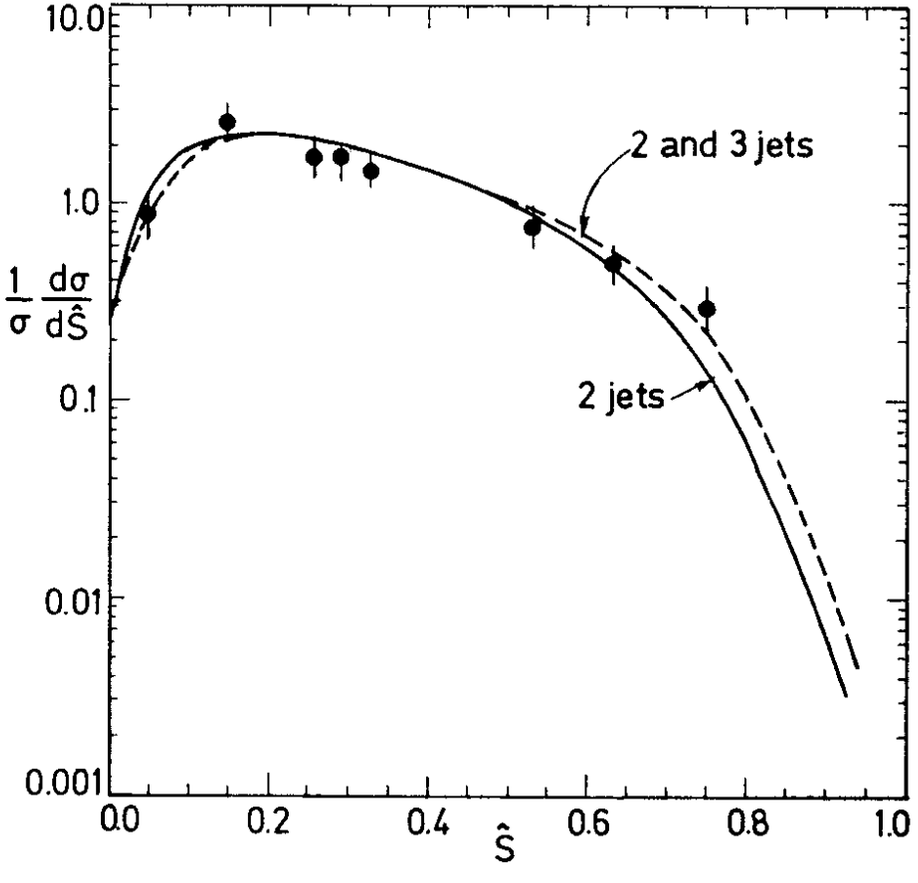

Fig.10a

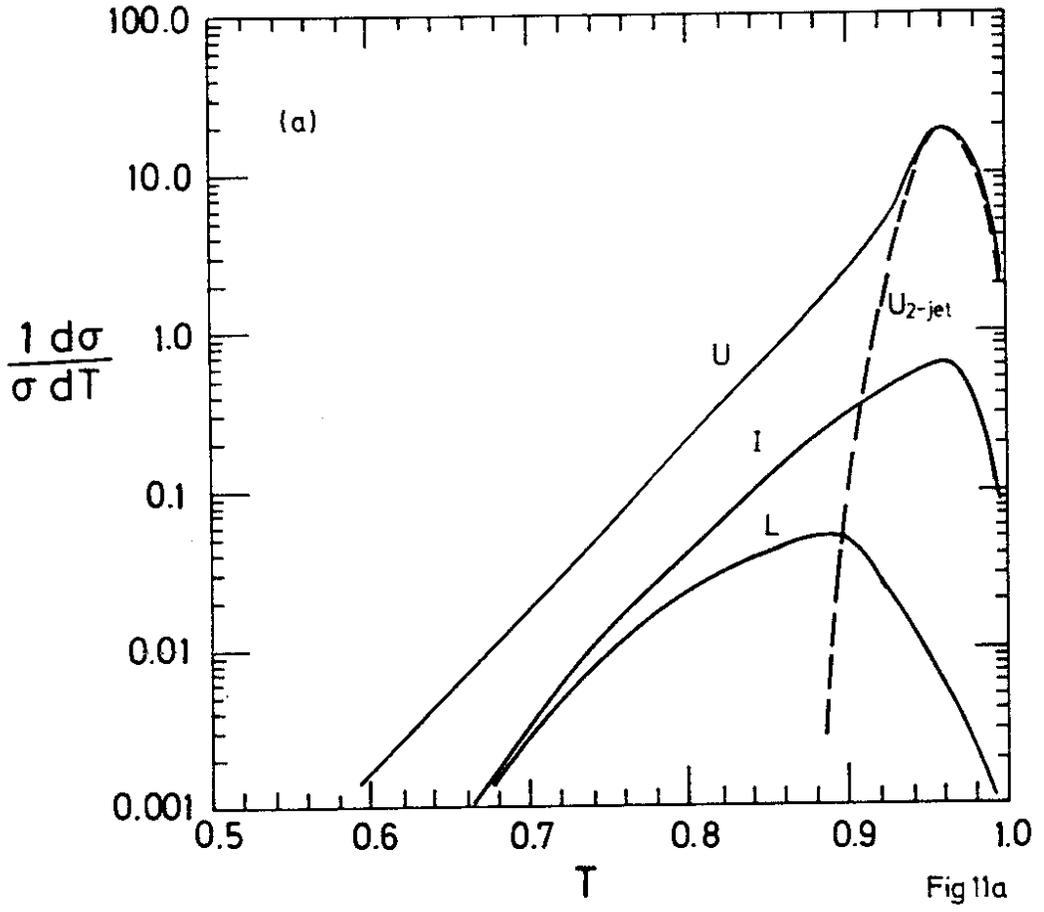

Fig 11a

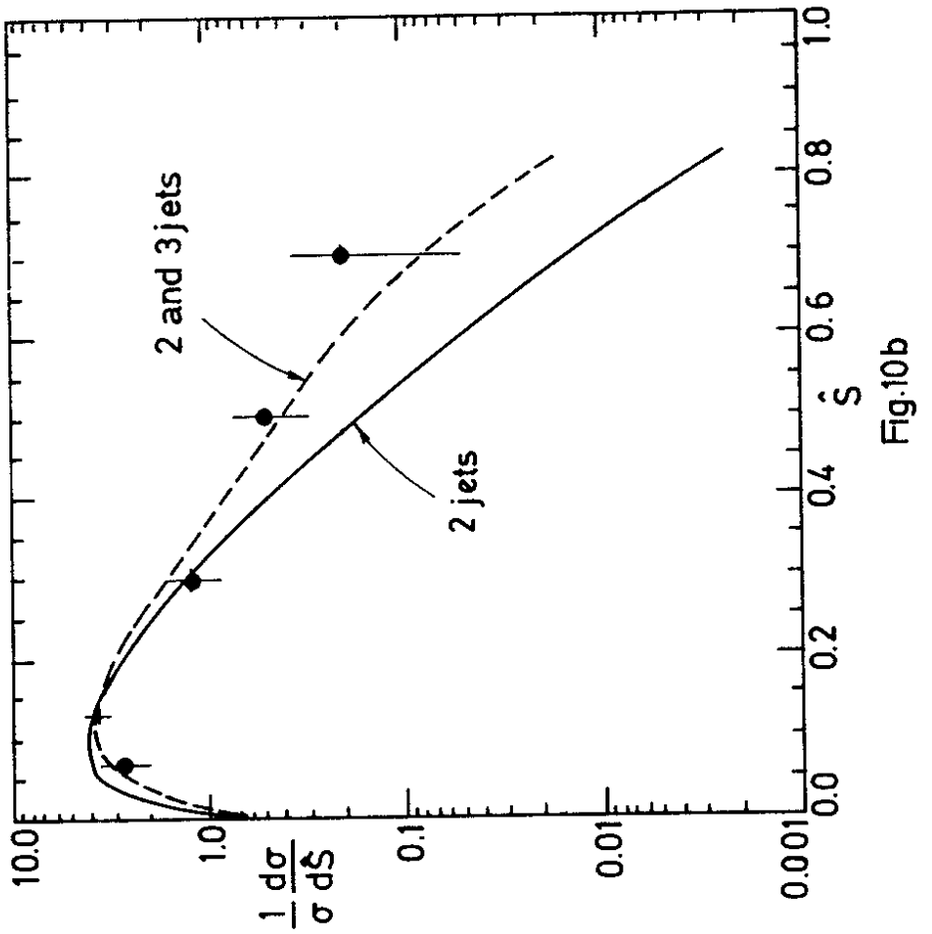

Fig.10b

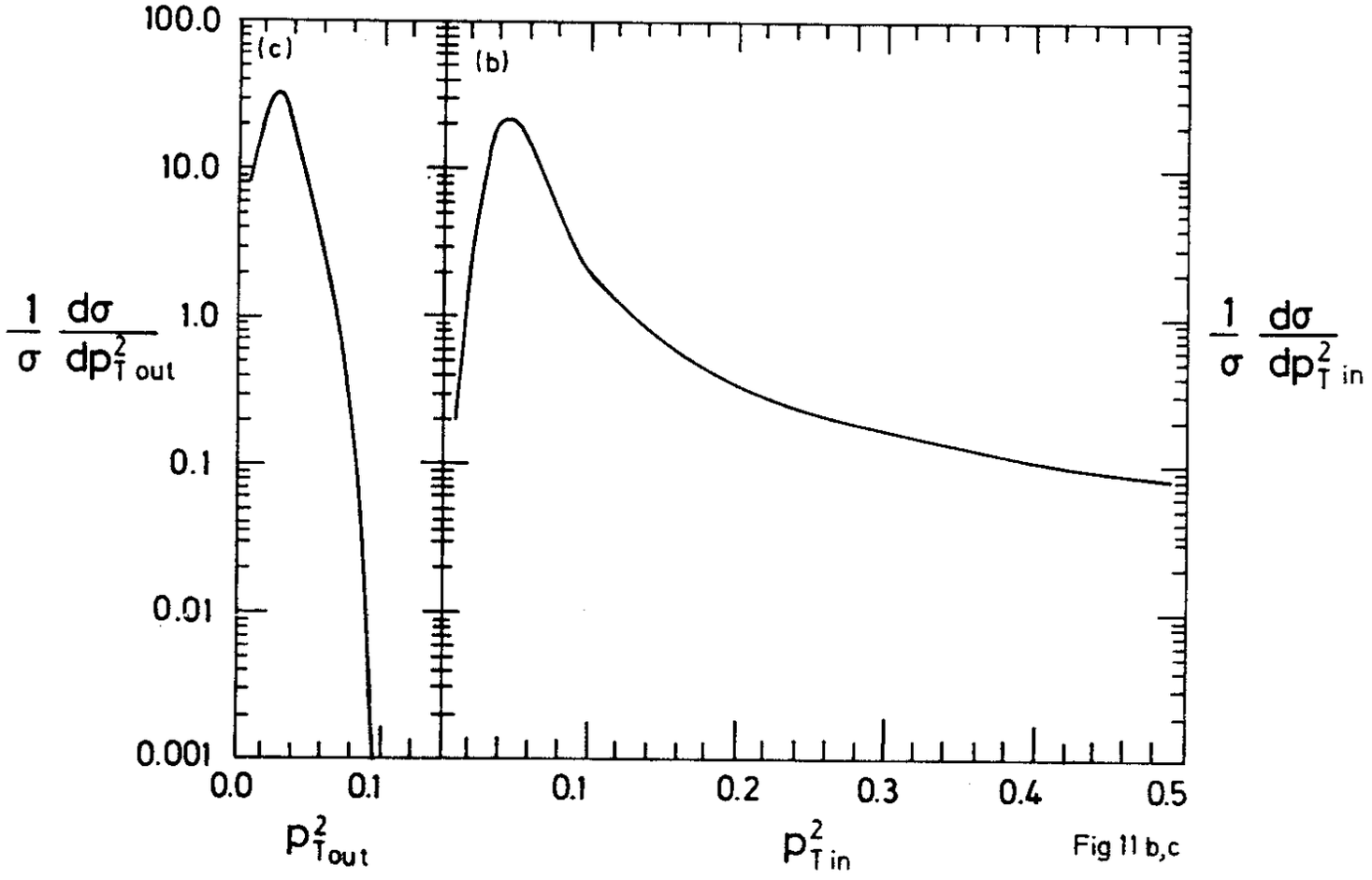

Fig 11 b,c

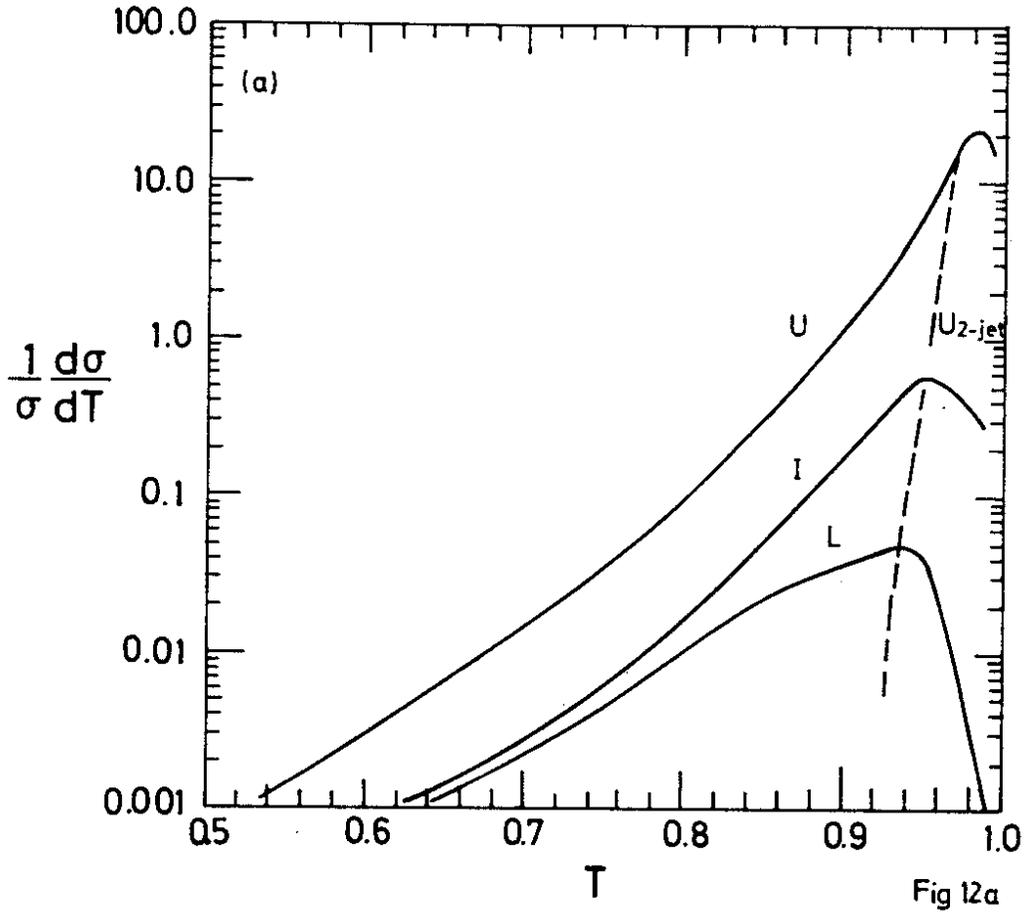

Fig 12a

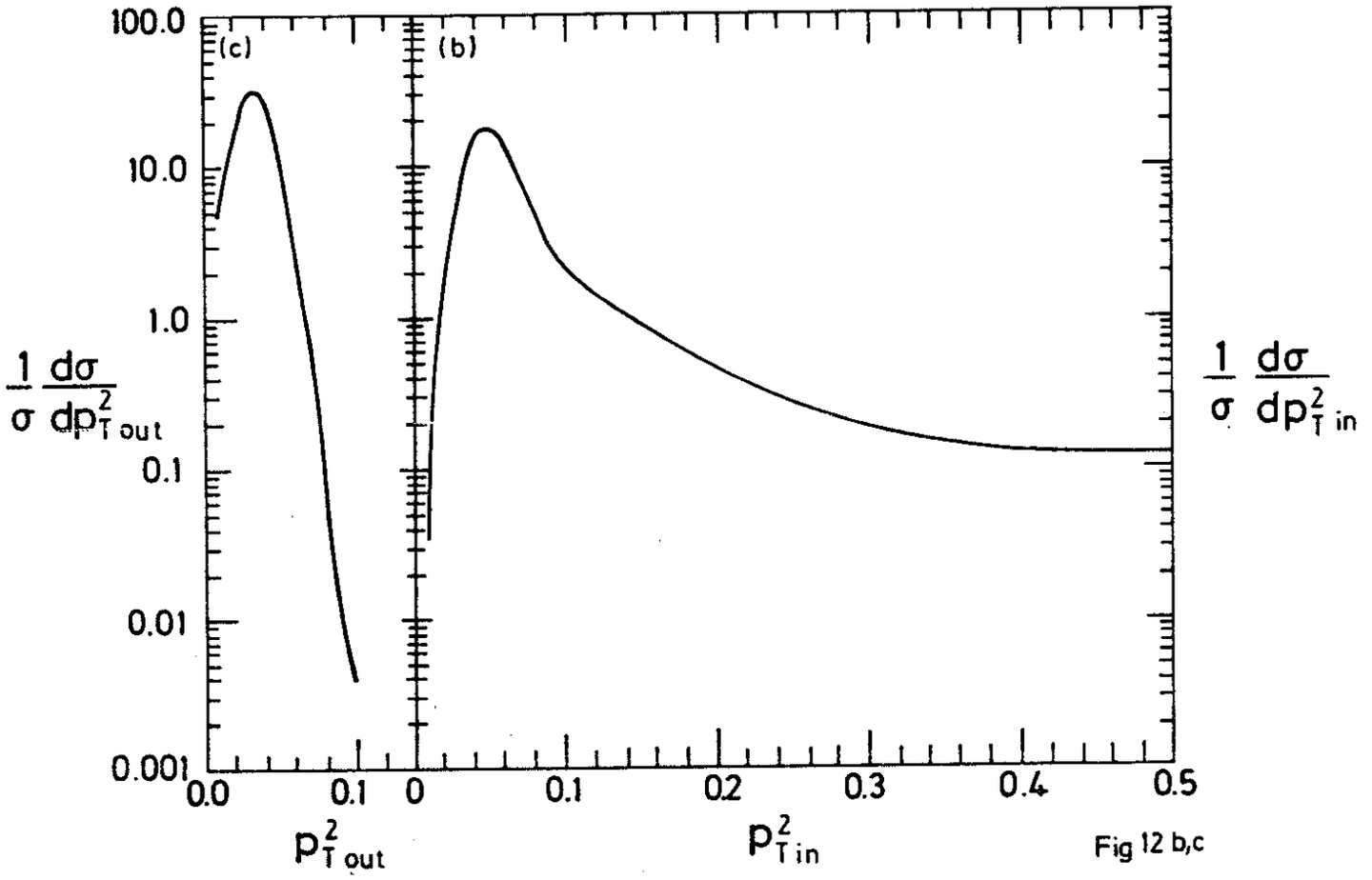

Fig 12 b,c

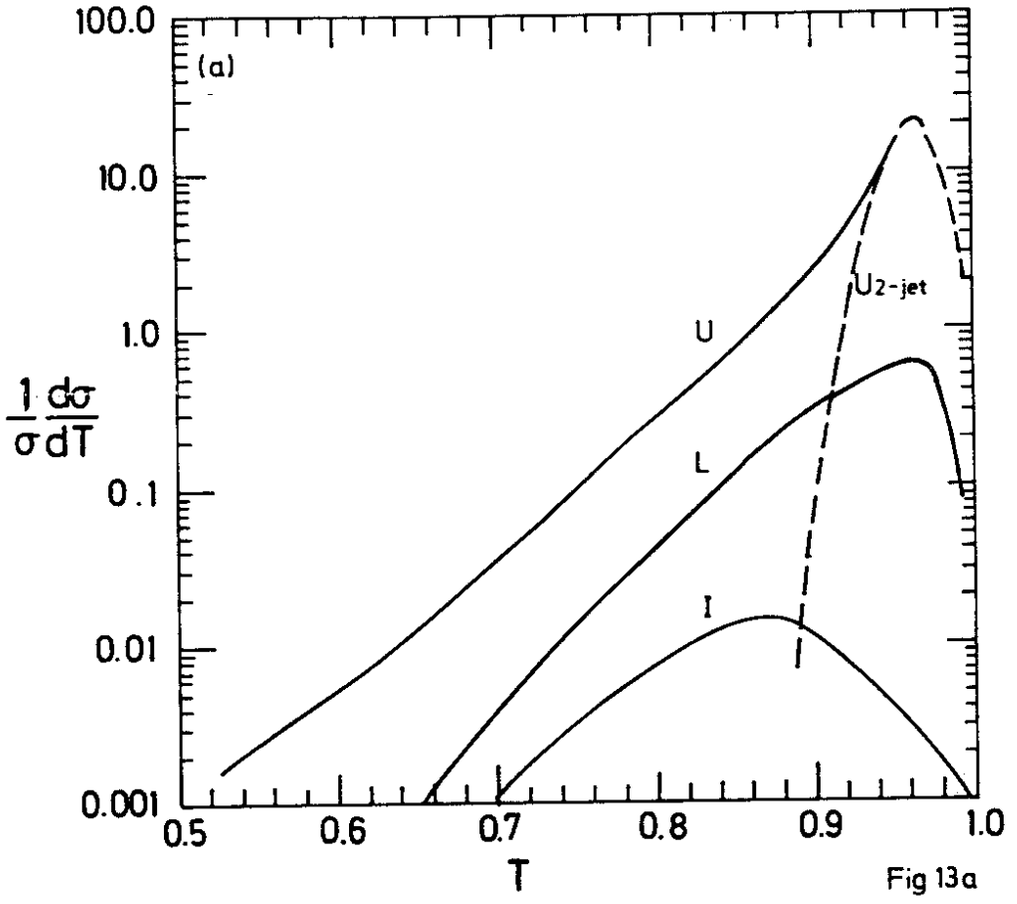

Fig 13a

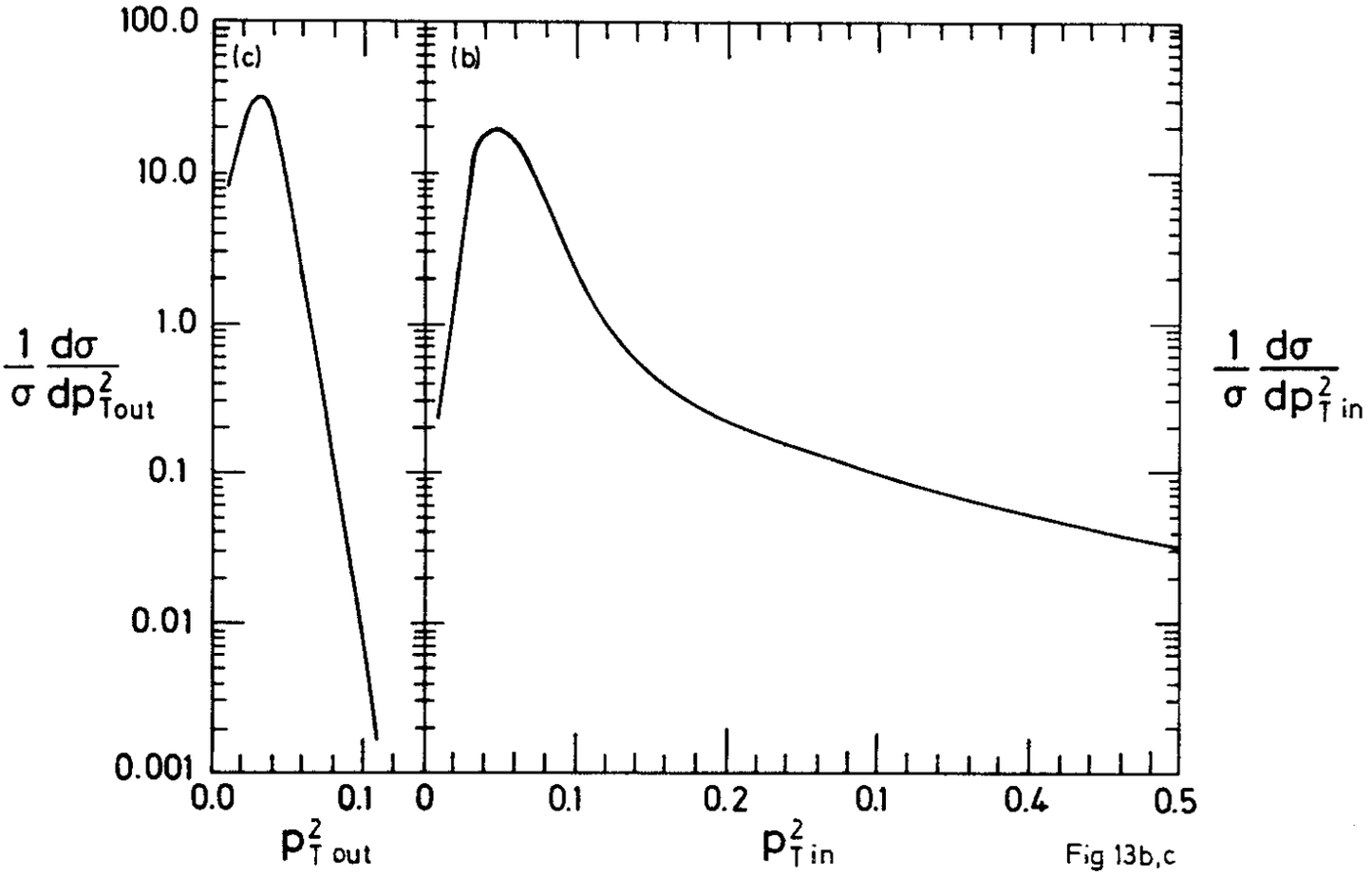

Fig 13b,c

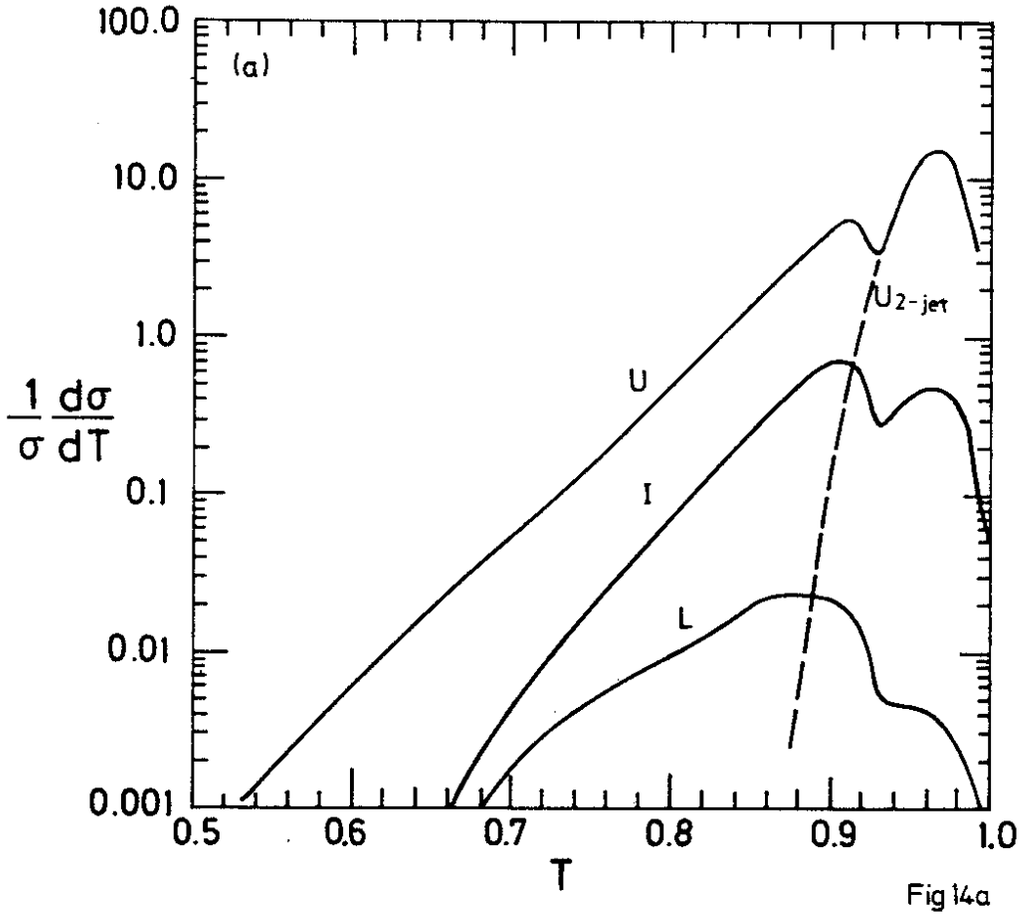

Fig 14a

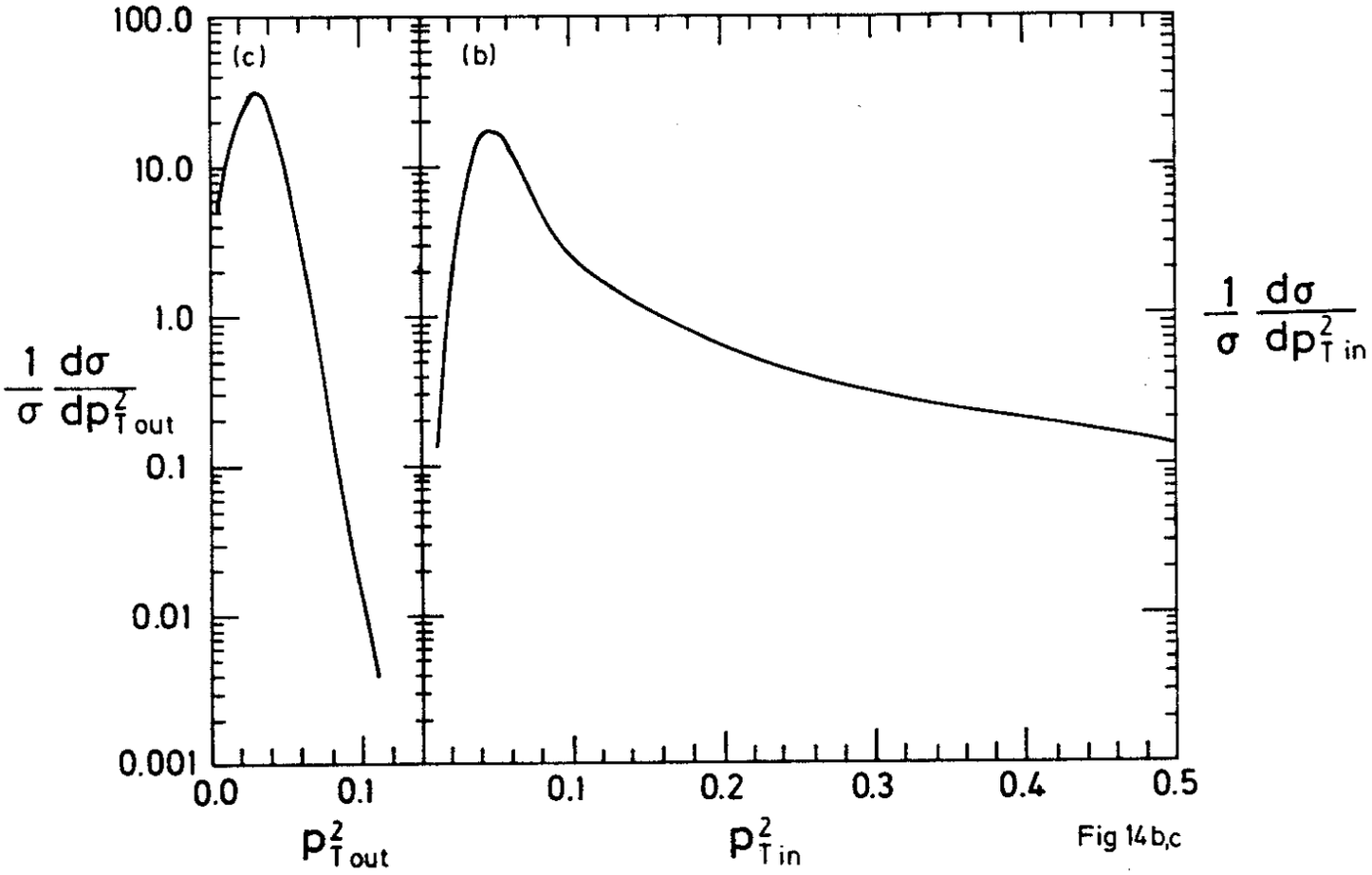
100.0
10.0
1.0
0.1
0.01
0.001
(c)
(b)
0.0
0.1
0.1
0.2
0.3
0.4
0.5
$\frac{1}{\sigma}\frac{d\sigma}{dp^2_{T\,out}}$
$\frac{1}{\sigma}\frac{d\sigma}{dp^2_{T\,in}}$
$p^2_{T\,out}$
$p^2_{T\,in}$

Fig 14 b,c